Neurobiology of Disease 182 (2023) 106142

Contents lists available at ScienceDirect

Neurobiology of Disease

journal homepage: www.elsevier.com/locate/ynbdi

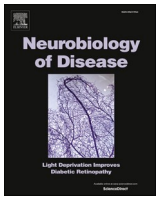

BACE cleavage of APP does not drive the diabetic phenotype of PLB4 mice

Z.J. Franklin, L. Croce, R. Dekeryte, M. Delibegovic, B. Platt *

Institute of Medical Sciences, School of Medicine, Medical Sciences & Nutrition, Foresterhill, University of Aberdeen, Aberdeen AB25 2ZD, Scotland, UK

ARTICLE INFO

Keywords:
Alzheimer's disease
Beta-secretase
Amyloid Beta
Type 2 diabetes mellitus
Insulin
Glucose
Ageing

ABSTRACT

Background: Alzheimer's Disease (AD) and Type 2 Diabetes Mellitus (T2DM), two prevalent diseases related to ageing, often share common pathologies including increased inflammation, endoplasmic reticulum (ER) stress, and impaired metabolic homeostasis predominantly affecting different organs. Therefore, it was unexpected to find in a previous study that neuronal *h*BACE1 knock-in (PLB4 mouse) leads to both an AD- and T2DM- like phenotype. The complexity of this co-morbidity phenotype required a deeper systems approach to explore the age-related changes in AD and T2DM-like pathologies of the PLB4 mouse. Therefore, we here analysed key neuronal and metabolic tissues comparing associated pathologies to those of normal ageing.

Methods: Glucose tolerance, insulin sensitivity and protein turnover were assessed in 5-h fasted 3- and 8-month-old male PLB4 and wild-type mice. Western Blot and quantitative PCR were performed to determine regulation of homeostatic and metabolic pathways in insulin-stimulated brain, liver and muscle tissue.

Results: Neuronal *h*BACE1 expression caused early pathological cleavage of APP (increased monomeric Aβ (mAβ) levels at 3 months), in parallel with brain ER stress (increased phosphorylation of the translation regulation factor (p-eIF2α) and the chaperone binding immunoglobulin protein (BIP)). However, APP processing shifted over time (higher full-length APP and secreted APPβ levels, alongside lower mAβ and secreted APPα at 8 months), together with increased ER stress (phosphorylated/total inositol-requiring enzyme 1α (IRE1α)) in brain and liver. Metabolically, systemic glucose intolerance was evident from 3 months, yet metabolic signalling varied greatly between tissues and ages, and was confined to the periphery (increased muscle insulin receptors (IR), dipeptidyl-peptidase-4 (DPP4) levels, and decreased phosphorylated protein Kinase B (p-Akt), alongside increased liver DPP4 and fibroblast growth factor 21 (FGF21)), all of which normalised to wild-type levels at 8 months.

Conclusion: Our data suggest that the murine nervous system is affected early by APP misprocessing as a result of *h*BACE1 introduction, which coincided with ER stress, but not IR changes, and was alleviated with age. Peripheral metabolic alterations occurred early and revealed tissue-specific (liver vs. muscle) adaptations in metabolic markers but did not correlate with neuronal APP processing. Compensatory vs. contributory neuronal mechanisms associated with *h*BACE1 expression at different ages may explain why mice intrinsically do not develop AD pathologies and may offer new insights for future interventions.

1. Introduction

Chronic diseases associated with age are increasingly affecting our ageing populations, with two of the most prevalent diseases being Alzheimer's Disease (AD) and Type 2 diabetes (T2DM). AD, the most prevalent cause of dementia, is characterised by a progressive decline in cognitive function, memory loss and changes in personality. Key pathological features comprise tau-based neurofibrillary tangles and the cleavage products of the amyloid precursor protein (APP). Here, beta secretase 1 (BACE1) is the rate-limiting enzyme resulting in beta-amyloid (Aβ) production and the subsequent formation of oligomeric and fibrillar Aβ species (Koss et al., 2016; Vassar et al., 1999). Epidemiological and molecular evidence provides insight into common pathological mechanisms and comorbidities associated with Alzheimer's Disease related dementias (ADRDs) and T2DM, most of which have been attributed to the role of insulin in neuronal physiology and

Abbreviations: T2DM, Type 2 diabetes mellitus; GTT, glucose tolerance test; ITT, insulin tolerance test.

* Corresponding author at: Chair in Translational Neuroscience, School of Medicine, Medical Sciences & Nutrition, University of Aberdeen, Foresterhill, Aberdeen AB25 2ZD, Scotland, UK.

E-mail address: b.platt@abdn.ac.uk (B. Platt).

https://doi.org/10.1016/j.nbd.2023.106142
Received 29 January 2023; Received in revised form 26 April 2023; Accepted 29 April 2023
Available online 1 May 2023

metabolism as well as inflammatory pathways (Arnold et al., 2018; Griffith et al., 2018; Li et al., 2015).

Growing evidence supports a link between T2DM, cognitive impairment and ADRDs. A higher degree of cognitive impairment in older individuals was associated with poor glycaemic control and also in individuals with a longer duration of T2DM. Furthermore, cognitive impairment and structural changes in the brain have been identified in younger individuals with T2DM. These data suggest that both cerebrovascular and age-related neurodegeneration, and early disease processes may play a part in ADRD's pathogenesis (Arnold et al., 2018). Transgenic models of T2DM have reported the development of pathologies such as Aβ plaques, tau hyperphosphorylation and α-synuclein, key pathologies in ADRDs (Ke et al., 2009; Kimura, 2016). Conversely, no positive associations between T2DM and AD pathologies have been observed in post-mortem human samples, however associations have been established between T2DM and cerebrovascular disease. These post-mortem studies do not account for the time course of disease, where pathologies of T2DM may contribute to ADRD's preclinical asymptomatic stages. Furthermore, compelling evidence suggests that normal brain metabolism and insulin signalling are essential for healthy brain ageing, cognition, and mood (Arnold et al., 2018).

Our previous work has shown that neuron-specific expression of human BACE1 (*h*BACE1, PLB4 mouse) results in both AD and T2DM phenotypes, including cognitive impairment, hyperglycaemia, and impaired peripheral insulin signalling (Plucińska et al., 2014, 2016). However, the exact interplay between metabolic regulation and APP processing remained unclear.

Numerous studies have demonstrated that BACE1 is associated with an increased risk of developing diabetes. Indeed, BACE1 levels and activity have been observed in patients with T2DM: elevated levels correlated with glycaemic status and BACE1-mediated insulin receptor cleavage is associated with insulin resistance (Bao et al., 2021). BACE1 is also expressed in many metabolically active cell types including pancreatic β-cells, adipocytes, hepatocytes, and vascular cells where elevated levels are implicated in T2DM, obesity, and cardiovascular disease development (Taylor et al., 2022). Reducing BACE1 activity in the periphery, specifically in liver and skeletal muscle (BACE1 knockout or pharmacological inhibition), can improve metabolic phenotypes associated with T2DM, including improved glucose tolerance and insulin sensitivity (Dekeryte et al., 2021; Meakin et al., 2012). Furthermore, altered APP processing and the APP metabolite sAPPβ have been shown to regulate skeletal muscle glucose uptake and impair insulin signalling, which are essential regulators of muscle glucose homeostasis (Botteri et al., 2018; Hamilton et al., 2014), and indicate strong associations between APP processing, peripheral glucose homeostasis and metabolic regulation.

BACE1 levels and activity generally increase with age and in conditions of cellular stress, and there is growing evidence that the increase in BACE1 levels itself as well as resultant APP metabolites activate the endoplasmic reticulum stress (ER) response, increase inflammation, and impair insulin signalling (Ghemrawi and Khair, 2020; Plucińska et al., 2014). As the cellular organelle involved in protein folding, translation and transport, disruptions in ER homeostasis and subsequent chronic activation of the 'unfolded protein response' can lead to the accumulation of misfolded proteins, cellular dysfunction, and ultimately cell death (Koss and Platt, 2017; Özcan et al., 2004, 2006). Metabolic dysregulation, including hyperglycaemia, insulin resistance and impaired insulin signalling, occurs in multiple peripheral tissues, including liver and muscle, also triggering ER stress responses. Conversely, chronic activation of ER stress affects glucose metabolism (Back and Kaufman, 2012; Huang et al., 2019).

A second common denominator implicated in both AD and T2DM pathology is the activation of the inflammasome (Zhai et al., 2018). 'NLR family pyrin domain containing 3' (NLRP3) is a sensor molecule, which alongside the adaptor protein apoptosis-associated speck-like protein containing a caspase recruitment domain (ASC) and pro-caspase-1, forms the inflammasome. When activated, this processes pro-interleukin 1 Beta (pro-IL1β) into mature IL1β, a key regulator of inflammatory cell death (Wang et al., 2020). Inhibition of NLRP3 reduced Aβ accumulation and improved cognitive function in APP/PS1 mice (Dempsey et al., 2017). Importantly, the NLRP3 inflammasome is also involved in peripheral glucose homeostasis where human studies have indicated that increased NLRP3 expression is associated with insulin resistance and hyperglycaemia. Furthermore, hyperinsulinemia and insulin resistance can increase the inflammasome response in the liver (Rai et al., 2020; Rheinheimer et al., 2017).

Another emerging metabolic regulator of interest is Dipeptidyl peptidase-4 (DPP4), due to its role in the inflammatory response during metabolic dysregulation. DPP4, a serine protease that inactivates incretin hormones involved in the regulation of glycaemia, also cleaves and deactivates cytokines and chemokines involved in inflammation and immune responses (Klemann et al., 2016). Serum DPP4 is increased in the neuronal *h*BACE1 knock in (PLB4) mouse, and inhibition of DPP4 improved glycaemic control and cognitive function in elderly diabetic patients with and without AD (Dekeryte et al., 2019; Isik et al., 2017).

Overall, these findings suggest that despite the multitude of pathways and tissues involved in the pathogenesis of both AD and T2DM there are striking similarities and associations that can influence both disease states alone, and in co-morbid phenotypes.

Here, we sought to further characterise the role of neuronal *h*BACE1 expression in the onset and progression of the co-morbid AD and T2DM-like phenotypes using the PLB4 model as a tool to investigate changes in key tissues involved in AD and T2DM pathologies including the brain, liver, and muscle. We investigated in detail molecular mechanisms and signalling pathways involved in APP processing, insulin signalling, ER stress. and inflammation and examined how these pathways may be involved in amyloid pathogenesis vs. metabolic dysregulation in young-adult (3-month-old) and older (8-month-old) male PLB4 and wild-type (WT) mice.

2. Materials and methods

2.1. Animals

Three- and eight-month-old PLB_{WT} and PLB4 male mice (PLB_{WT} 3 months, $n = 12$; PLB_{WT} 8 months $n = 6$; PLB4 3 months $n = 10$; PLB4 8 months $n = 6$) were generated as previously described (Plucińska et al., 2014). Animals were bred at Charles River UK on a C57BL/6 J background where PLB4 lines are regularly refreshed and maintained according to their inbred colony management practices including backcrossing genetic lines with wild-type congenic rodents from the supplier. Animals were housed in wire top cages in a climate-controlled holding room (20–21 °C, 60–65%, relative humidity), with a 12-h day/night cycle (lights on at 7 am) and ad libitum access to food and water. All animals were tested in accordance with the European directive 63/2010E and UK Home Office Regulations and the Animal (Scientific Procedures) Act 1986 and conducted according to the ARRIVE guidelines 2.0 for reporting animal research (du Sert et al., 2020). Testing order between genotypes were randomised (www.random.org), and the experimenter was blinded to the genotype of the subject. Power calculations were not available; therefore, estimates were based on previous research (Dekeryte et al., 2019, 2021; Plucińska et al., 2016). All mice were 5-h fasted and humanely culled by cervical dislocation (without the use of anaesthesia to ensure minimum distress of the animals, and to exclude interference with tissue readouts) at the end of the study.

2.2. Glucose and insulin tolerance tests

Glucose and insulin tolerance tests were performed in 5-h fasted mice as per our previous studies (Dekeryte et al., 2021). Body weights and fasting blood glucose were measured prior to intraperitoneal (i.p.)

injection of glucose (2 mg/g body weight, D-glucose Sigma, UK) or insulin (0.75 U/kg body weight, Humulin R, Eli Lilly), and blood glucose levels measured at 0-, 15-, 30-, 60- and 90-min post-injection using an AlphaTrak glucometer (Berkshire, UK).

2.3. Tissue preparation

Three and eight-month-old mice were fasted for 5-h and randomised to receive an i.p. injection of insulin (10 U/kg body weight, PLB_{WT} 3 months: $n = 6$, PLB4 3 months: $n = 6$, PLB_{WT} 8 months $n = 5$, PLB4 8 months: $n = 5$) 10 min prior to being humanely culled by cervical dislocation (Dekeryte et al., 2021). Brain, liver, and muscle tissue were dissected, snap frozen in liquid nitrogen, and stored at −80 °C. Brain tissue was homogenised manually using a pestle in NP-40 lysis buffer (final concentration: 20 mM N2-hydroxyethylpiperazine-N′-2-ethanesulphonic acid (HEPES), 150 mM sodium chloride (NaCl), 100 μM ethylenediaminetetraacetic acid (EDTA), 1% IGEPAL (CA-630), pH 7.6). Liver and muscle tissue were homogenised using a mechanical homogeniser in RIPA lysis buffer (10 mM tris(hydroxymethyl)aminomethane hydrochloride (Tris-HCl), 150 mM NaCl, 0.1% sodium dodecylsulphate (SDS), 1% Triton X-100, 1% sodium deoxycholate, 5 mM EDTA, 1 mM sodium fluoride (NaF), 1 mM sodium orthovanadate (NaOV), pH 7.4). Lysis buffers were supplemented with complete protease inhibitors (1 tablet/10 ml, cat# 11836145001, Roche, Sigma, UK) and PhosStop tablets (1 tablet/10 ml, cat# 4906837001, Roche, Sigma, UK). Tissue homogenates were centrifuged (12,000 rpm, 20 min, 4 °C) and supernatants collected and stored at −80 °C.

2.4. Immunoblotting

Insulin-stimulated brain, muscle, and liver sample protein concentrations were determined using a Bicinchonic Acid (BCA) protein assay (cat# BCA1-1KT, Sigma, UK). Brain samples were prepared at a final concentration of 3 μg/μl in NP40 buffer, and muscle or liver samples were prepared at 2-3 μg/μl in RIPA buffer containing lithium dodecyl sulphate (LDS, cat# 15484379, Thermo Fisher Scientific, UK), 15 mM dithiothreitol (DTT, cat# 10197777001, Sigma, UK), and heated to 70 °C for 10 min. Samples were randomised for gel loading and proteins separated by electrophoresis on NuPage 4–12% sodium Bistris gels for 45 min in 3-(N-morpholino)propanesulphonic acid (MOPS) buffer, and were transferred via wet transfer onto 0.45 μm nitrocellulose membranes at 25 V for 1-h at room temperature.

For detection of the APP metabolites sAPPα, sAPPβ and C-terminal fragments 83 and 99 (CTF83 and CTF99), brain samples were prepared at 3 μg/μl in NP40 containing LDS, 15 mM DTT, and heated to 70 °C for 10 min. To detect full-length APP (FL-APP) and monomeric beta-amyloid (Aβ), brain samples were prepared at 3 μg/μl in NP40 containing LDS, however DTT was omitted, and samples were not heated prior to gel electrophoresis due to the sensitivity of Aβ species under denaturing conditions (Koss et al., 2016). Proteins were separated by gel electrophoresis at 200 V for 30 min in 2-(NMorpholino)ethanesulfonic acid (MES) buffer and transferred using the Nu Page IBlot transfer system (ThermoFisher Scientific) onto 0.2 μm nitrocellulose membranes at 23 V for 6 min. Following protein transfer membranes for FL-APP and mAβ were microwaved in 2 × 1.5 min 0.01 M phosphate buffer saline (PBS, cat# P4417, Sigma, UK).

Following transfer, membranes were blocked in 5% milk Tris-buffered saline with Tween (TBST: 0.05% Tween-20, 50 mM Tris base, 150 mM NaCl, pH 7.6 using 2 M HCl) for 1-h at room temperature and subsequently washed 3 × 10 min in TBST. Membranes were incubated overnight at 4 °C in primary antibodies prepared in TBST containing 5% BSA and 0.05% sodium azide (Supplementary Table 1). Following incubation, membranes were washed 3 × 5 min in TBST and incubated in appropriate secondary antibodies (Supplementary Table 1).

2.5. Protein quantification

Proteins were visualised by enhanced chemiluminescence using a Vilber-Fusion camera and Fusion Software (PEQLAB, Germany). Proteins were quantified via analysis of area under the curve (AUC) 16bit Western Blot images using ImageJ software and total protein loading determined by Coomassie Blue stain (Plucińska et al., 2014). All markers were normalised to total protein and expressed relative to 3 month wild-type animals. The number of independent samples run per antibody are stated in each figure legend. All samples were run over at least two gels. Raw images for Western Blots can be found in Supplementary Fig. 1.

2.6. Puromycin assay

Three- and eight-month-old male PLB_{WT} (3 months: $n = 7$, 8 months: $n = 5$) and PLB4 (3 months: $n = 12$, 8 months: $n = 11$) mice were anaesthetised and administered unilateral intracerebroventricular injections of puromycin (25 mg/2.0 ml, Sigma, UK) or vehicle (artificial cerebrospinal fluid, aCSF with 10% DMSO), coordinates: −2 mm anterioposterior, 2 mm mediolateral, and 1.5 mm dorsoventral), as described previously (Hull et al., 2020). Mice were humanely culled by cervical dislocation 2-h post injection and half brains dissected for total protein extraction. Puromycin incorporation was detected using an anti-puromycin antibody (1:500, Millipore, UK) via Western blots as described in Section 2.4.

2.7. Quantitative polymerase chain reaction (qPCR)

Total RNA was extracted from insulin-stimulated half brain and liver tissue using the TRIzol method. Briefly, 50-100 mg frozen tissue was pulse homogenised in 1 ml TRI Reagent (Sigma, UK), and tissue homogenates incubated at room temperature for 5 min to allow for nucleoprotein complexes to completely dissociate from RNA. Chloroform was added to homogenates (200 μl/1 ml TRI Reagent), vortexed and samples incubated at room temperature (RT) for 15 min. Samples were centrifuged (12,000 *g*, 15 min, 4 °C) allowing for phase separation. Following centrifugation, the aqueous phase was collected into fresh nuclease free tubes, 250 μl of isopropanol (Sigma, UK) was added, and samples were incubated at −20 °C overnight to allow for RNA precipitation. Samples were again centrifuged (12,000 *g*, 15 min, RT), supernatant removed, and the RNA pellet washed in 75% ethanol. Ethanol was removed, RNA pellets were air dried and dissolved in Tris-EDTA. RNA was quantified using a NanoDrop 1000A system (Thermo Scientific, USA). cDNA was synthesised from 3 to 5 μg total RNA using a Bioline cDNA synthesis kit (Bioline, London, UK). Total RNA was combined with (per sample): 0.5 μl Oligo (dT)18, 0.5 μl Random Hexamer, 10 mM dNTP mix, 5xRT Buffer (final concentration 1×), 1 u/μl Ribosafe RNase Inhibitor, 200u/μl Reverse Transcriptase and DEPC-treated water, and reverse transcription performed (25 °C for 10 min, 45 °C for 30 min, 85 °C for 5 min, 4 °C (infinite hold)) in a BioRad T100 ThermalCycler (BioRad, UK). Target genes were amplified from 0.3 to 0.5 μg cDNA by qPCR using GoTaq Master Mix (Promega, Southampton, UK) in a Roche LightCycler 480 (Roche Diagnostics, Burgess Hill, UK). Relative gene expression was calculated using the Ct method ($2 - \delta\delta Ct$), and the geometric mean of the three most stable reference genes (*Rn18s, Ywhaz, Nono*) were used to normalise data. Data were expressed as fold change relative to 3-month-old wild-type controls. Primer sequences used for gene expression analysis are listed in Supplementary Table 2.

2.8. Statistical analysis

All statistical analysis and graphs were prepared using GraphPad Prism V8.0 (GraphPad, USA). Data normality was probed using the Shapiro-Wilk normality test and outliers determined based on the Grubb's (3 standard deviations from mean) outlier test. Data were averaged by genotype and age, and represented as mean ± SD. For all

data sets, alpha was set to 5% and p values < 0.05 were considered significant. Full statistical analyses are provided in Supplementary Tables 3–20.

2.8.1. Glucose and insulin tolerance tests

A 2-way analysis of variance (ANOVA) was performed for baseline blood glucose, insulin tolerance tests, and area under or above the curve (AUC or AAC) analysis to determine main effects and interactions for genotype (PLB4 vs. PLB_{WT}) and age (3- vs. 8 months), followed by Tukey's multiple comparisons post-hoc analysis. A two-tailed unpaired t-test with Welch's correction was performed for baseline blood glucose and AUC / AAC analyses where only two groups were compared. Main effects and interactions for glucose tolerance tests were assessed by 3-way repeated measures (RM) ANOVA for genotype (PLB4 vs. PLB_{WT}), age (3- vs. 8 months), and time (RM) followed by Tukey's multiple comparisons to determine age or genotype specific changes within each time point (0–90 min).

2.8.2. Molecular data analysis

Protein levels (Western Blot) and gene expression (qPCR) data were analysed by 2-way ANOVA to assess main effects and interactions for genotype (PLB4 vs. WT) and age (3- vs. 8 months), followed by Tukey's multiple comparison post-hoc analysis to determine genotype specific effects within age, or age specific effects within genotype.

2.8.3. Correlation analysis

Correlation analysis was carried out within brain, muscle, and liver tissue, and between brain, muscle, and liver tissue for all protein and genetic markers of interest. Data underwent Z-score transformation and were assessed for normal distribution using D'Agostino & Pearson normality test followed by Pearson r correlation coefficient analysis. Pearson r- values were used to determine positive ($r > 0.7$) or negative correlations ($r < -0.7$) between markers and between tissues. Correlations were deemed significant if $p < 0.05$ and are displayed in a heat plot matrix with blue indicating positive correlations and red indicating negative correlations.

3. Results

3.1. APP processing

Our previous studies have shown that the neuron-specific knock-in of *h*BACE1 results in a diabetic-like phenotype alongside AD-relevant changes in 6-month-old PLB4 mice (Dekeryte et al., 2021; Plucińska et al., 2016). Therefore, we first assessed AD markers and age-related changes in APP processing in the PLB4 mouse model in young (3-month-old) and aged (8-month-old) PLB4 mice and compared with age-matched wild-types (WT). Protein levels of full-length APP (FL-APP) and secreted-APPβ (sAPPβ) were significantly increased only in the brain of 8-month-old PLB4 animals compared to 8-month-old WT controls (FL-APP genotype: $F(1, 17) = 8.18$; $p = 0.0108$, PLB4 8 months vs. WT 8 months: $p = 0.0224$, Fig. 1A), (sAPPβ interaction: $F(1, 18) = 6.899$; $p = 0.0171$, genotype: $F(1, 18) = 4.874$; $p = 0.0405$, PLB4 8 months vs. WT 8 months: $p = 0.0201$, Fig. 1E), alongside lower secreted-APPα (sAPPα) levels (genotype: $F(1, 17) = 15.26$; $p = 0.0011$, age: $F(1, 17) = 16.18$; $p = 0.0009$, interaction: $F(1, 17) = 10.00$; $p = 0.0057$, PLB4 8 months vs. WT 8 months: $p = 0.0007$, PLB4 8 months vs. PLB4 3 months: $p = 0.0004$, Fig. 1B). FL-APP, sAPPα and sAPPβ were not altered in 3-month-

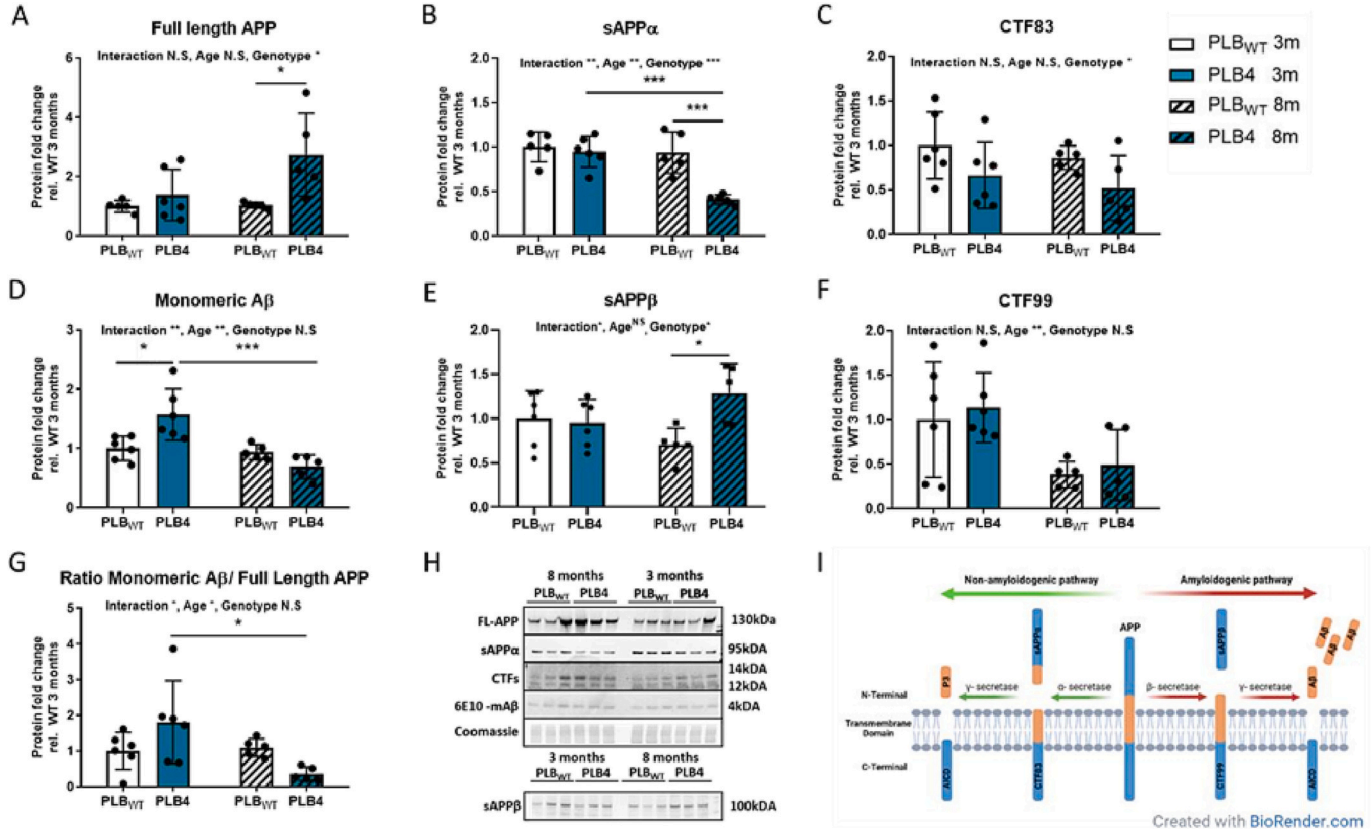

Fig. 1. APP processing in insulin-stimulated brain tissue of 3- and 8-month-old PLB4 and PLB_{WT} mice. Quantification of protein levels of (A) full-length APP, (B) sAPPα, (C) CTF83, (D) monomeric Aβ, (E) sAPPβ, (F) CTF99, (G) the ratio of monomeric Aβ/full length APP, determined via Western blotting. (H) Representative western blots for APP processing markers. (I) Diagram showing the normal and pathological processing of APP. Data were quantified as fold change relative to 3-month-old PLB_{WT}, expressed as means ± SD and analysed using two-way ANOVA, followed by Tukey's multiple comparison test. $^*p < 0.05$, $^{**}p < 0.01$, $^{***}p < 0.001$. PLB_{WT} 3 months ($n = 6$), PLB4 3 months ($n = 6$), PLB_{WT} 8 months ($n = 5$), PLB4 8 months ($n = 5$). For full statistical results, see Supplementary Tables.

old PLB4 mice compared to their controls ($p > 0.05$, Fig. 1A, B & E). Further analysis revealed no age-specific significant changes in the C-terminal fragments (CTF) CTF83 and CTF99 protein levels in PLB4s compared to WT controls ($p > 0.05$, Fig. 1C & F), although there was an overall genotype effect indicating lower CTF83 protein levels in PLB4 animals (genotype: F (1, 18) = 5.60; $p = 0.0293$). For CTF99, an age-dependent reduction was observed in both groups (age: F (1, 18) = 10.90; $p = 0.0040$, Fig. 1F).

Interestingly, genotype-specific and age-related changes in monomeric Aβ levels were detected in PLB4 mice only at 3 months, where PLB4s had increased monomeric Aβ protein levels compared to WT controls and 8-month-old PLB4 mice (interaction: (F (1, 18) = 12.04; $p = 0.0027$, age: (F (1, 18) = 15.82; $p = 0.0009$, PLB4 3 months vs. WT 3 months: $p = 0.0103$, PLB4 3 months vs. PLB4 8 months: $p = 0.0003$, Fig. 1D). However, 8-month-old PLB4 mice did not show changes in monomeric Aβ protein levels compared to their WT counterparts ($p > 0.05$, Fig. 1D). Despite there being no genotype-specific effect in the ratio of monomeric Aβ to FL-APP, an overall age effect was observed, i.e. PLB4 animals had a lower FL-APP/monomeric Aβ ratio at 8 months compared to 3-month-old PLB4 animals (interaction: F (1, 18) = 6.81; $p = 0.0177$, age: F (1, 18) = 5.25; $p = 0.0343$, PLB4 3 months vs. PLB4 8 months: $p = 0.0134$, Fig. 1G). Overall, our data indicate age-dependent alterations in APP processing in PLB4 mice, indicative of amyloidogenic processing at 3 months, yet a shift in APP cleavage by both BACE1 and α-secretase at 8 months.

3.2. Glucose tolerance

Systemic glucose tolerance was also assessed in the same animals. As in previous studies, PLB4 mice displayed elevated fasted baseline glucose levels compared to WT controls (genotype effect: F (1, 28) = 41.48; $p < 0.0001$, 3 months: $p < 0.0001$, 8 months: $p = 0.0009$, Fig. 2A). Impaired glucose clearance was also observed in PLB4 mice (genotype effect: F (1, 27) = 64.45; $p < 0.0001$, time x genotype: F (4, 108) = 6.175; $p = 0.0002$), with blood glucose levels significantly elevated in 3-month-old PLB4's at 15-, 30-, 60- and 90-min post i.p. glucose injection (15–60 min: $p < 0.0001$, 90 mins: $p = 0.0418$), and in 8-month-old PLB4 mice at 15 and 60 mins (15 mins: $p = 0.0145$, 60 mins: $p = 0.0447$, Fig. 2B). Total glycaemic excursion as determined by AUC was also significantly elevated in PLB4 animals compared to WT (genotype: F (1, 28) = 45.68; $p < 0.0001$, 3 months: $p < 0.0001$, 8 months: $p = 0.0073$, Fig. 2C) following a 5-h fasted GTT. No significant effect of ageing on glucose clearance was observed between 3- and 8-month-old WT or PLB4 mice, indicating glucose clearance in PLB4 animals is impaired from 3 months and ageing does not alter this metabolic impairment (baseline glucose age: F (1, 28) = 2.114; $p = 0.1571$, GTT age: F (1, 27) = 1.803; $p = 0.1905$, AUC age: F (1, 28) = 0.7322; $p = 0.3994$, Fig. 2C). Neuronal *h*BACE1 did not affect plasma glucose responses to i.p. insulin in 3-month-old PLB4 mice (genotype: $p = 0.92$, AAC: $p = 0.76$, Fig. 2E & F).

3.3. Insulin signalling and glucose regulation in brain and peripheral tissues

3.3.1. Insulin signalling and glucose transport responses in the brain

To determine the effect of brain-specific insulin signalling on the diabetic phenotype observed in PLB4 animals, we carried out Western blot analysis of proteins related to insulin signalling in brain tissue of both 3- and 8-month-old mice. We did not detect major genotype-specific changes in the classical insulin signalling targets in the brain, i.e. there were no significant changes in total levels of the insulin receptor (IR), protein kinase B (Akt) and ribosomal protein S6 (rpS6) ($p > 0.05$, Fig. 3A & B). However, phosphorylated Akt was age-dependently increased only in WT animals (age: F (1, 18) = 16.60; $p = 0.0007$, WT 3 months vs. WT 8 months: $p = 0.0386$, Fig. 3A & B). Furthermore, phosphorylated rpS6 and the ratio of phosphorylated/total rpS6 were decreased with age in both WT and PLB4 mice (prpS6 age: F (1, 18) = 23.12; $p = 0.0001$, p/t-rpS6 age: F (1, 17) = 41.14; $p < 0.0001$, Fig. 3A & B). The glucose transporter type 4 (GLUT4), which facilitates transport of glucose into tissues for storage, also decreased with age in both WT and PLB4 animals (age: F (1, 18) = 29.17; $p < 0.0001$, Fig. 4A & B). Therefore, minor changes observed in brain insulin signalling and glucose transport appear to be a result of age rather than a consequence of neuronal *h*BACE1 expression.

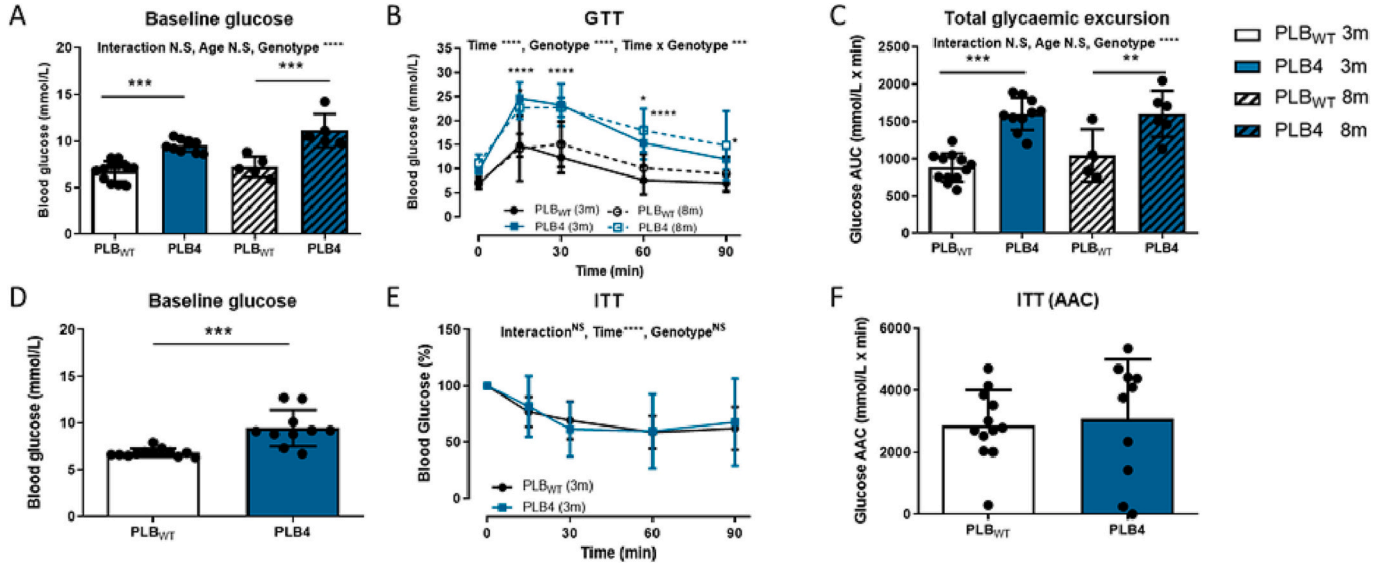

Fig. 2. Metabolic phenotype of 3- and 8-month-old male PLB4 and PLB$_{WT}$ mice. (A) Basal glucose levels, (B) glucose tolerance test (GTT), and (C) quantification of area under the curve (AUC) for total glycaemic excursions in 5-h fasted 3- and 8-month-old mice following 2 mg/g body weight i.p. glucose injection. (D) Baseline blood glucose levels, (E) insulin tolerance test (ITT), and (F) quantification of AAC analysis for ITT in 5-h fasted 3-month-old mice post 0.75 U/g body weight i.p. insulin injection. Data are expressed as means ± SD and analysed using 2-way ANOVAs for baseline glucose, AUC and ITT, two-tailed unpaired *t*-test with Welch's correction for baseline glucose and AAC with only two groups, and 3-way RM ANOVA for GTT analysis, followed by post-hoc analysis. *$p < 0.05$, **$p < 0.01$, ***$p < 0.001$, ****$p < 0.0001$. PLB$_{WT}$ 3 months ($n = 12$), PLB4 3 months ($n = 10$), PLB$_{WT}$ 8 months ($n = 6$), PLB4 8 months ($n = 6$). For full statistical results, see Supplementary Tables.

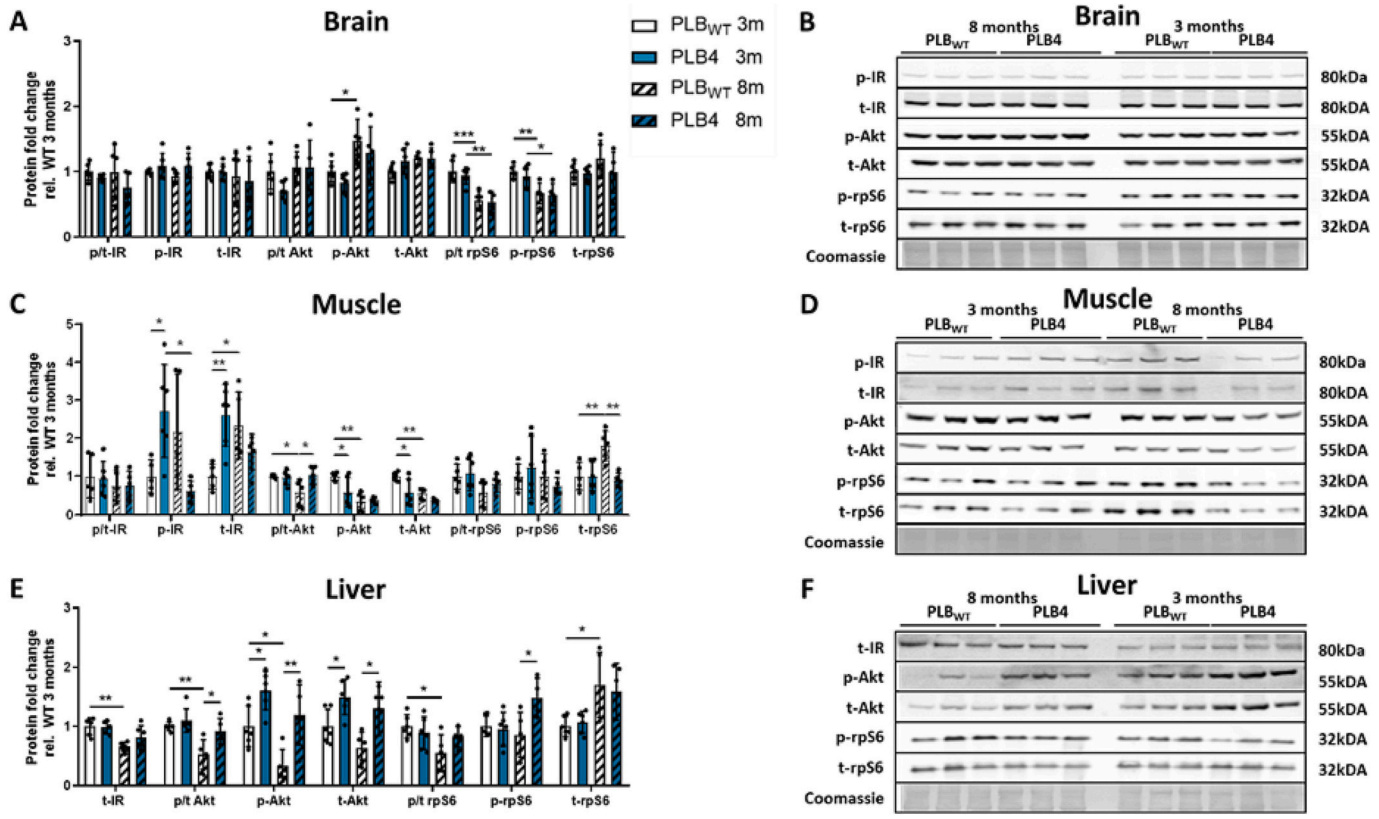

Fig. 3. Insulin signalling in insulin-stimulated brain and peripheral tissues of 3- and 8-month-old PLB4 and PLB_{WT} mice. Protein levels as determined by Western blot of total, phosphorylated and the ratio of phosphorylated/total IR, Akt, and rpS6 in the (A) brain, (C) muscle, and (E) liver following insulin stimulation in 3- and 8-month-old PLB_{WT} and PLB4 mice. Representative Western blots of insulin signalling markers in the (B) brain, (D) muscle, and (F) liver. Proteins were normalised to total Coomassie stain, and phosphorylated markers were normalised to their respective total proteins. Data are expressed as fold change relative to 3-month-old PLB_{WT} ± SD, and analysed using two-way ANOVA, followed by Tukey's multiple comparison test. $^{*}p < 0.05$, $^{**}p < 0.01$. PLB_{WT} 3 months ($n = 6$), PLB4 3 months ($n = 6$), PLB_{WT} 8 months ($n = 5$), PLB4 8 months ($n = 5$). For full statistical results, see Supplementary Tables.

3.3.2. *Insulin signalling and glucose transport responses in muscle*

Skeletal muscles are the primary site of energy expenditure and the main site of glucose storage (as glycogen), and insulin-stimulated glucose disposal is impaired in T2DM. In contrast to the limited changes in brain markers regulating insulin signalling and glucose transport in PLB4 animals, pronounced IR-related changes were detected in muscle tissue. Total and phosphorylated IR (post insulin stimulation) were significantly increased in 3-month-old PLB4 animals (total-IR interaction: F (1, 17) = 15.17; $p = 0.0012$, PLB4 3 months vs. WT 3 months: $p = 0.005$) (p-IR interaction: F (1, 17) = 13.87; $p = 0.0017$, PLB4 3 months vs. WT 3 months: $p = 0.0494$) and total and phosphorylated Akt was lower in 3-month-old PLB4s compared to WT controls (t-Akt genotype: F (1, 18) = 11.64; $p = 0.0031$, age: F (1, 18) = 14.33; $p = 0.0014$, PLB4 3 months vs. WT 3 months: $p = 0.0110$), (p-Akt interaction: F (1, 18) = 4.663; $p = 0.0446$, age: F (1, 18) = 16.49; $p = 0.0007$, PLB4 3 months vs. WT 3 months: $p = 0.0356$, Fig. 3C & D). Changes in insulin signalling components observed in 3-month-old PLB4 mice were not observed in 8-month-old PLB4s (PLB4 vs. WT: $p > 0.05$, Fig. 3C & D).

Furthermore, age-related changes were seen only in WT controls including increased total IR (WT 3 months vs. WT 8 months: $p = 0.0293$), increased total rpS6 (interaction: F (1, 17) = 9.437; $p = 0.0069$, genotype: F (1, 17) = 9.271; $p = 0.0073$, age: F (1, 17) = 5.390; $p = 0.0329$, WT 3 months vs. WT 8 months: $p = 0.0081$), and decreased total Akt, phosphorylated Akt and the ratio of phosphorylated/total Akt (WT 3 months vs. WT 8 months: t-Akt: $p = 0.0080$, p-Akt: $p = 0.0018$, p/t-Akt: $p = 0.0226$) in 8-month-old WT compared to 3-month-old WT (Fig. 3C & D). In contrast, the only age-related changes observed in muscle of PLB4 mice was a decrease in phosphorylated/total Akt and an increase in total rpS6 compared to 8 month WT controls (p/t-Akt interaction: F (1, 18) = 6.730; $p = 0.0183$, genotype: F (1, 18) = 5.41; $p = 0.0318$, PLB4 8 months vs. WT 8 months: $p = 0.0177$) (t-rpS6 genotype: F (1, 17) = 9.271; $p = 0.0073$, PLB4 8 months vs. WT 8 months: $p = 0.0028$, Fig. 3C & D). Secondly, phosphorylated IR protein levels decreased significantly with age in PLB4s while it revealed a trend to increase in the control WT cohort (p-IR PLB4 8 months vs PLB4 3 months: $p = 0.0140$, Fig. 3C & D). Despite the increase in IR levels of PLB4 mice at 3 months, no genotype specific differences in GLUT4 protein were observed, only an overall age effect was obtained (age: F (1, 18) = 4.759; $p = 0.0426$, Fig. 4A & B). Hence, it would appear that upregulation of glucose uptake was not achieved in young PLB4 mice, despite higher IR levels, in line with the sustained diabetic phenotype.

Overall, key metabolic changes involved in insulin signalling that occur naturally with age were not observed in PLB4s, alongside considerable changes present in 3-month-old PLB4 mice, which suggests that this pathway is dysregulated early in PLB4s, and the maturation profile seen in WTs is not recapitulated in PLB4 mice.

3.3.3. *Insulin signalling and glucose metabolism in the liver*

The liver is crucial for gluconeogenesis, second in line for glycogen storage, and key regulator of energy and nutrient metabolism. Here, insulin signalling was affected in both 3- and 8-month-old PLB4 mice. Genotype and age significantly altered Akt protein regulation: total and phosphorylated Akt levels were increased in PLB4 animals compared to age-matched controls (t-Akt genotype: F (1, 18) = 18.77; $p = 0.0004$, PLB4 3 months vs. WT 3 months: $p = 0.0465$, PLB4 8 months vs. WT 8 months: $p = 0.0209$), (p-Akt genotype: F (1, 18) = 21.33; $p = 0.0002$, age: F (1, 18) = 11.55; $p = 0.0032$, PLB4 3 months vs. WT 3 months: $p = 0.0496$, PLB4 8 months vs. WT 8 months: $p = 0.0086$, Fig. 3E & F).

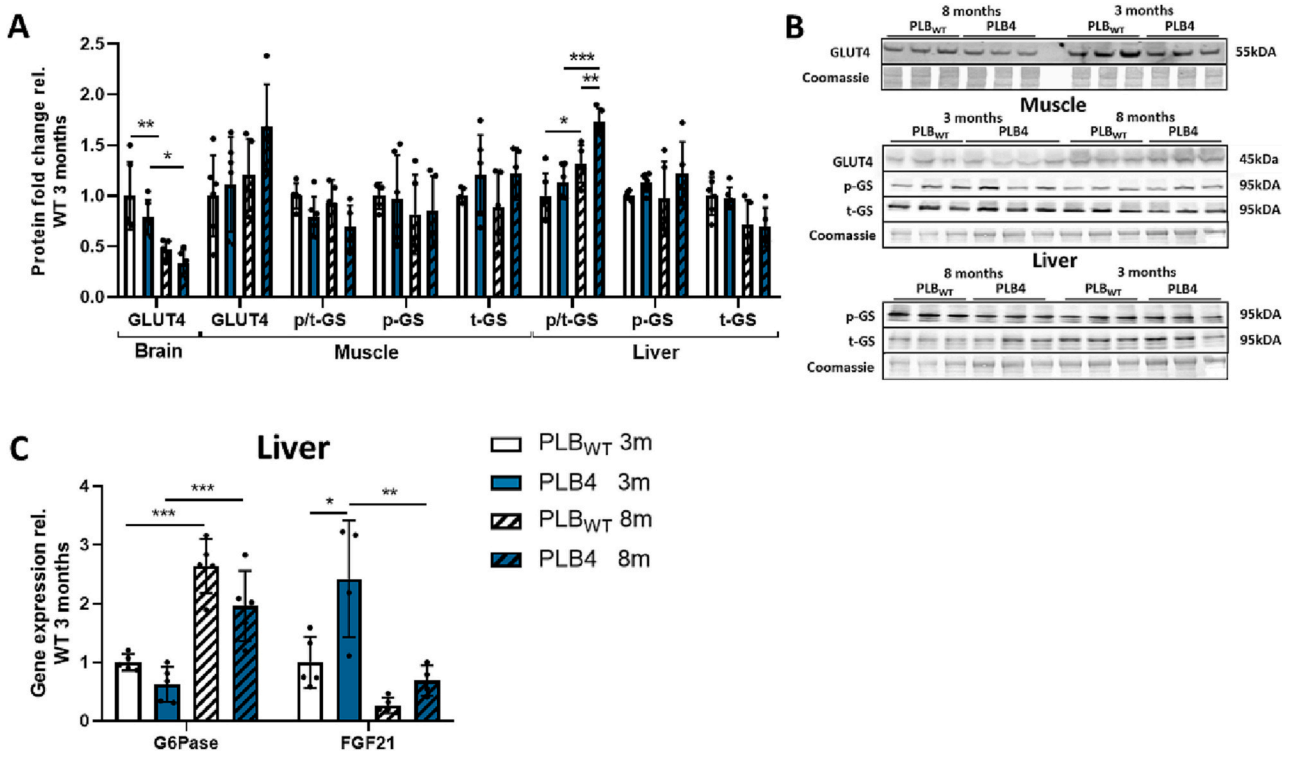

Fig. 4. Gene expression and protein analysis of glucose regulatory markers in insulin-stimulated brain and peripheral tissues of 3- and 8-month-old PLB4 and PLB$_{WT}$ mice. (A) Western blot quantification of GLUT4 and glycogen synthase in the brain, muscle and liver of PLB$_{WT}$ and PLB4. (B) Representative Western blots of GLUT4, total, phosphorylated, and the ratio of phosphorylated/total GS protein levels in brain, muscle and liver of PLB$_{WT}$ and PLB4s. (C) Gene expression of G6Pase and FGF21 in the liver of PLB$_{WT}$ and PLB4 animals. Proteins were normalised to Coomassie total protein and phosphorylated markers normalised to their respective total protein concentrations. Protein and gene expression data are expressed as fold change relative to 3-month-old PLB$_{WT}$ ± SD, and analysed using two-way ANOVAs, followed by Tukey's multiple comparison test. *$p < 0.05$, **$p < 0.01$, ***$p < 0.001$. PLB$_{WT}$ 3 months ($n = 6$), PLB4 3 months ($n = 6$), PLB$_{WT}$ 8 months ($n = 5$), PLB4 8 months ($n = 5$). For full statistical results, see Supplementary Tables.

Furthermore, 8-month-old PLB4s also displayed an increased ratio of phosphorylated/total Akt (genotype: F (1, 18) = 9.22; $p = 0.0071$, age: F (1, 18) = 16.10; $p = 0.0008$, PLB4 8 months vs. WT 8 months: $p = 0.0189$), and increased phosphorylated rpS6 compared to their age-matched WT controls (interaction: F (1, 17) = 5.681; $p = 0.0291$, PLB4 8 months vs. WT 8 months: $p = 0.0464$, Fig. 3E & F).

Conversely, WT animals exhibited a different insulin signalling maturation profile compared to PLB4 animals. Unfortunately, the antibody used here successfully for other tissues did not detect phosphorylated IR in the liver of either genotype, however there was a significant age-associated decrease in protein levels of total IR (age: F (1, 19) = 19.24; $p = 0.0003$, WT 3- vs. 8 months: $p = 0.0022$), phosphorylated Akt, and the ratio of phosphorylated/total Akt in WT controls, which was not the case in PLB4 animals (p-Akt WT 3 months vs. WT 8 months: $p = 0.0022$, p/t-Akt WT 3 months vs. WT 8 months: $p = 0.0032$, Fig. 3E & F). Furthermore, total rpS6 and the phosphorylated/total rpS6 ratio were increased and decreased, respectively, in WT animals, another change which was not observed in PLB4 animals (t-rpS6 age: F (1, 18) = 14.90; $p = 0.0011$, WT 3 months vs. WT 8 months: $p = 0.0257$), (p/trpS6 age: F (1, 17) = 5.373; $p = 0.0332$, WT 3 months vs. WT 8 months: $p = 0.0350$, Fig. 3E & F).

In addition to post-insulin receptor signalling markers, protein levels and gene expression of metabolic modulators were also determined. We have previously shown that hepatic glycogen levels are lower in PLB4 animals (Plucińska et al., 2016), therefore, we measured glycogen synthase (GS), a key enzyme involved in the conversion of glucose to glycogen. In line with the above metabolic data, GS levels were altered by age and genotype in the liver (t-GS age: F (1, 18) = 13.07; $p = 0.0020$, p/t-GS age: F (1, 18) = 34.63; $p < 0.0001$, p/t-GS genotype: F (1, 18) = 12.39; $p = 0.0024$, Fig. 4A & B). Furthermore, 8-month-old PLB4 mice had an increased ratio of phosphorylated/total GS in the liver compared to 3-month-old PLB4 and 8-month-old WT (PLB4 8 months vs. PLB4 3 months: $p = 0.0002$, PLB4 8 months vs. WT 8 months: $p = 0.0448$, Fig. 4A & B). Glycogen synthase is inactive in its phosphorylated form; therefore, the increased ratio of phosphorylate/total GS suggests reduced glycogen production and storage in the liver, which likely contributed to the increased circulating glucose levels observed in PLB4 (Plucińska et al., 2016).

Further gene expression analyses of Glucose 6-phosphotase (G6Pase), an enzyme involved in gluconeogenesis, indicated an overall genotype and age effect in G6Pase expression, with post-hoc analysis also showing significantly increased levels with age (genotype: F (1, 16) = 8.115; $p = 0.0116$, age: F (1, 16) = 64.94; $p < 0.0001$, PLB4 3 vs. 8 months: $p = 0.0005$, WT 3 vs. 8 months: $p < 0.0001$, Fig. 4C), while evidence for early metabolic dysregulation in PLB4 mice was indicated by enhanced expression of fibroblast growth factor 21 (FGF21). FGF21 is primarily a hepatokine involved in the regulation of metabolic processes such as insulin sensitivity and glucose metabolism in the liver; but also acts on a number of other tissues (Fisher and Maratos-Flier, 2016; Tezze et al., 2019). Furthermore, increased FGF21 levels in non-alcoholic fatty liver disease can overcome toxicity (Rusli et al., 2016). Here, liver FGF21 was significantly increased in 3-month-old PLB4s compared to WT controls; but decreased with age in PLB4 mice (genotype: F (1, 14) = 13.21; $p = 0.0027$, PLB4 3 months vs. WT 3 months: $p = 0.0068$, age: F (1, 14) = 23.66; $p = 0.0003$, PLB4 8 months vs. PLB4 3 months: $p = 0.0021$, Fig. 4C). No age-related changes in FGF21 gene expression were observed in WT animals suggesting this change was PLB4 specific (Fig. 4C).

3.4. ER stress response and inflammation in brain and peripheral tissues

3.4.1. Age- and genotype-specific changes in the ER stress response in the brain

Protein and gene expression analysis of ER stress markers, ER chaperones and inflammatory markers were assessed next in the brain of both 3- and 8-month-old PLB4 mice. Overall, genotype-specific changes in ER stress responses were detected. BIP protein levels and eIF2α phosphorylation were increased in 3-month-old PLB4 mice (BIP genotype: $F(1, 17) = 20.81$; $p = 0.0003$, PLB4 3 months vs. WT 3 months: $p = 0.0019$), (p-eIF2α genotype: $F(1, 18) = 15.27$; $p = 0.0010$, age: $F(1, 18) = 7.91$; $p = 0.0115$, PLB4 3 months vs. WT 3 months: $p = 0.0350$, Fig. 5B), while 8-month-old PLB4 mice displayed elevated levels in the ratio of phosphorylated to total IRE1α compared to their respective WT controls (interaction: $F(1, 18) = 6.23$; $p = 0.0225$, genotype: $F(1, 18) = 6.165$; $p = 0.0231$, PLB4 8 months vs. WT 8 months: $p = 0.0164$, Fig. 5B).

When comparing 3- and 8-month-old animals, ageing resulted in overall elevated ATF6, ATF4 and CHOP gene expression in both genotypes (ATF6 age: $F(1, 16) = 7.79$; $p = 0.0130$, ATF4 age: $F(1, 16) = 26.92$; $p < 0.0001$, CHOP age: $F(1, 16) = 48.48$; $p < 0.0001$, Fig. 5A). Interestingly, post-hoc analysis revealed age-specific changes in the ER stress response in PLB4 animals that were not observed with age in WT controls. PLB4s at 8 months exhibited an increase in BIP gene expression alongside decreased CHIP expression (BIP interaction: $F(1, 16) = 6.43$; $p = 0.0220$, age: $F(1, 16) = 14.27$; $p = 0.0016$, PLB4 3 vs. 8 month: $p = 0.0200$), (CHIP age: $F(1, 16) = 15.71$; $p = 0.0011$, PLB4 3 month vs. 8 month: $p = 0.0100$, Fig. 5A). These data indicate that *h*BACE1 expression causes early ER stress changes aligned with APP misprocessing; but not IR levels, and a change in the ER stress signalling cascade that is different to the normal ageing profiles of controls, which may be related to changes in APP processing observed in PLB4 mice.

3.4.2. Tissue and genotype specific ER stress response signalling in the periphery

To determine peripheral changes in the ER stress response of PLB4 mice, we next analysed protein levels of ER stress markers in muscle and liver tissue. In muscle tissue, phosphorylated to total IRE1α ratio was altered in an overall age-dependent manner regardless of genotype (age: $F(1, 17) = 5.649$; $p = 0.0295$). However, similarities between brain and muscle ER stress responses were observed for eIF2α activation. An overall genotype effect of eIF2α phosphorylated/total ratio was detected in muscle tissue (genotype: $F(1, 17) = 4.776$; $p = 0.0431$, Fig. 5C), suggesting that metabolic and APP dysregulation in PLB4 mice may activate similar pathways in the brain and periphery. Interestingly, despite the key role of muscle tissue in metabolic regulation, we did not detect any other significant ER changes between genotypes or age in muscle (PLB4 vs. WT or 3 months vs. 8 months, respectively: $p > 0.05$, Fig. 5C). Neither WT nor PLB4 mice showed changes in any ER stress markers measured in muscle tissue (genotype and age: $p > 0.05$, Fig. 5C), which may indicate better resilience towards IR dysregulation.

In contrast, both age- and genotype-related changes in ER stress markers were observed in liver tissue. Similar to our observations in the ER stress response in the brain, 3-month-old PLB4 animals displayed

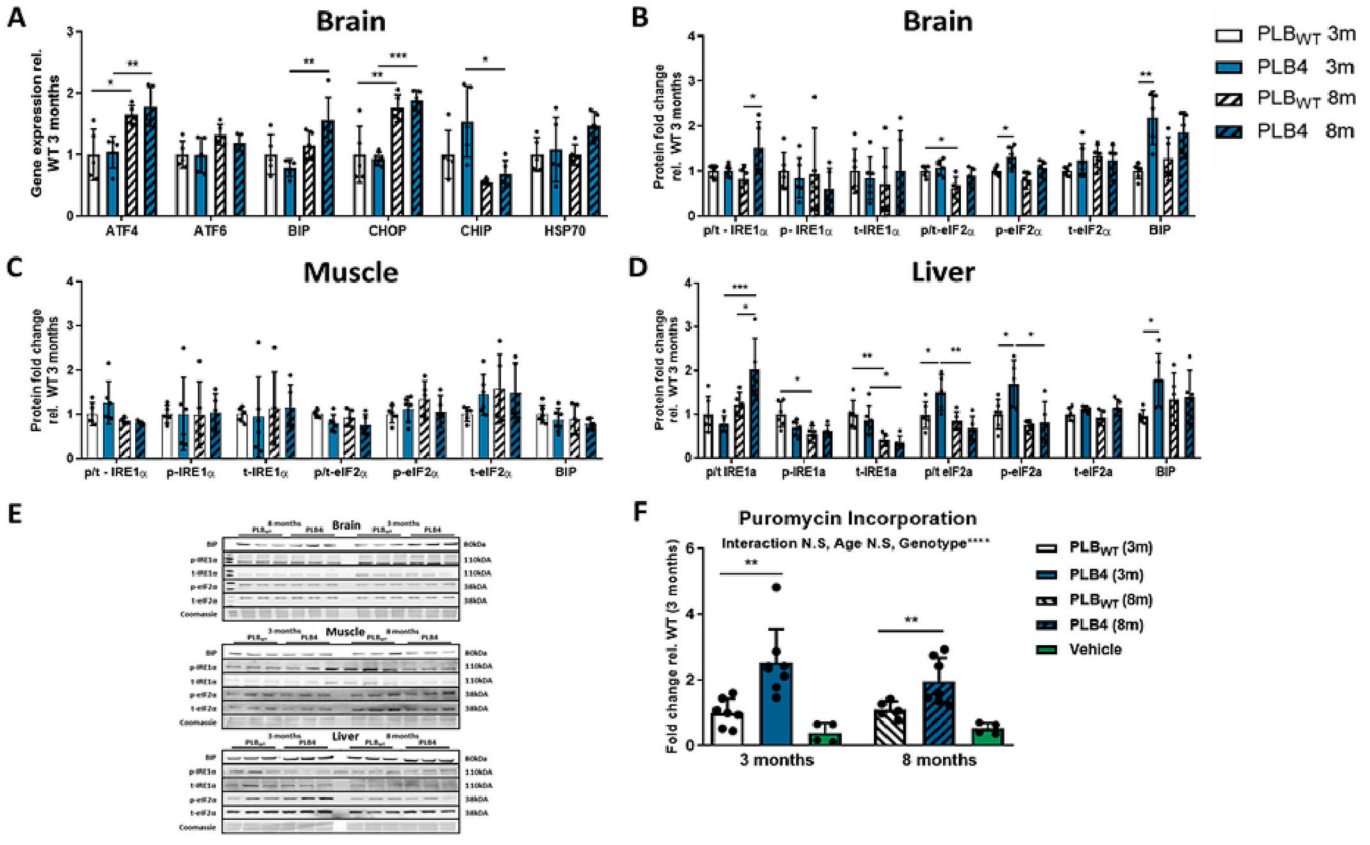

Fig. 5. ER stress and protein turnover in insulin-stimulated brain and peripheral tissues. Quantification of (A) gene expression and (B) protein levels of ER stress markers in the brain of 3- and 8-month-old PLB$_{WT}$ and PLB4 mice. Quantification of ER stress protein levels in (C) muscle and (D) liver tissues. (E) Representative Western blots of ER stress markers in the brain and peripheral tissues. (F) Western blot quantification of newly synthesised proteins (puromycin assay) in brain tissue of PLB4 mice at 3- and 8 months of age relative to PLB$_{WT}$ controls following ICV puromycin or vehicle (10% DMSO in aCSF) over a 2-h period. Total proteins were normalised to total Coomassie protein and phosphorylated markers normalised to their respective total proteins. Data are expressed as fold change relative to 3-month-old PLB$_{WT}$ ± SD, and analysed using two-way ANOVA, followed by Tukey's multiple comparison test. *$p < 0.05$, **$p < 0.01$, ***$p < 0.001$. PLB$_{WT}$ 3 months ($n = 6$), PLB4 3 months ($n = 6$), PLB$_{WT}$ 8 months ($n = 5$), PLB4 8 months ($n = 5$). For full statistical results, see Supplementary Tables.

increased BIP protein levels (genotype: F (1, 18) = 4.15; $p = 0.0565$, PLB4 3 months vs. WT 3 months: $p = 0.0492$), alongside increased eIF2α phosphorylation (genotype: F (1, 17) = 4.85; $p = 0.0418$, age: F (1, 17) = 10.70; $p = 0.0045$, PLB4 3 months vs. WT 3 months: $p = 0.0422$) and an increased phosphorylated/total eIF2α ratio (interaction: F (1, 17) = 6.93; $p = 0.0174$, age: F (1, 17) = 12.93; $p = 0.0022$, PLB4 3 months vs. WT 3 months: $p = 0.0486$) compared to their WT controls (Fig. 5D). Furthermore, 8-month-old PLB4 mice had an elevated phosphorylated/total IREα ratio compared age matched WT controls (interaction: F (1, 18) = 7.76; $p = 0.0122$, age: F (1, 18) = 16.18; $p = 0.0008$, PLB4 8 months vs. WT 8 months: $p = 0.0383$, Fig. 5D). Additional age-related changes in liver ER stress responses were also detected. PLB4 mice displayed genotype-specific changes in their ER stress response with ageing that were not observed in WT animals, including an increased ratio of phosphorylated/total IRE1α (age: F (1, 18) = 16.18; $p = 0.0008$, PLB4 3 months vs. PLB4 8 months: $p = 0.0007$), and a decreased ratio of phosphorylated/total eIF2α (genotype: F (1, 17) = 4.85; $p = 0.0418$, age: F (1, 17) = 10.70; $p = 0.0045$, PLB4 3 months vs. PLB4 8 months: $p = 0.0121$, Fig. 5B).

These data suggest that the above age-related and pathway-specific ER markers were altered only in PLB4 animals, while phosphorylated IRE1α only decreased in WT animals (age: F (1, 18) = 8.94; $p = 0.0078$, WT 3 months vs. WT 8- months: $p = 0.0105$), and total IRE1α decreased with age regardless of genotype (age: F (1, 18) = 24.93; $p < 0.0001$, Fig. 5D).

3.5. Protein turnover in the brain

Altered protein turnover rates are associated with age and an increased risk of amyloidosis; but also with dysregulated cellular signalling including the ER stress response (Hull et al., 2020; Patterson et al., 2015). Therefore, we used the puromycin (SunSet) assay, which measures protein synthesis *in vivo*, to compare the rate of brain protein turnover in WT and PLB4 animals (Goodman and Hornberger, 2013; Hull et al., 2020). Protein translation rates were increased in both 3-month-old (152%) and 8-month-old (78%) PLB4 mice compared to their age-matched controls (genotype: F (1,22) = 25.82; $p < 0.0001$, 3 months: $p = 0.0012$, 8 months: $p = 0.0411$, Fig. 5F), indicative of generally enhanced protein processing in PLB4 animals. This increase may be compensatory and aid the reversal of APP misprocessing with age.

3.6. Inflammasome signalling in brain and liver

The NLRP3 inflammasome is considered a sensor of changes in homeostasis and has been implicated in the pathogenesis of metabolic and neurodegenerative diseases. Western blot analysis of NLRP3 revealed that PLB4 animals had increased liver NLRP3 protein levels at 3 months of age (interaction: F (1, 17) = 5.197; $p = 0.0358$, genotype: F (1, 17) = 9.077; $p = 0.0078$, age: F (1, 17) = 27.43; $p < 0.0001$, PLB4 3 months vs. WT 3 months: $p = 0.0067$, Fig. 6C). NLRP3 in the brain of 3 month PLB4 animals was somewhat lower; but this narrowly missed significance (genotype: F (1, 18) = 4.354; $p = 0.0507$, age: F (1, 18) = 155.8; $p < 0.0001$, PLB4 3 months vs. WT 3 months: $p = 0.0507$, Fig. 6A). An age-dependent decrease in NLRP3 levels was observed in the brain of both WT and PLB4s (WT 8 months vs. 3 months: $p < 0.0001$, PLB4 8 months vs. PLB4 3 months: $p < 0.0001$, Fig. 6A), while NLRP3 protein levels in the liver returned to control levels with age in PLB4 animals (PLB4 8 months vs. PLB4 3 months: $p = 0.0004$, Fig. 6C). NLRP3 protein levels were not detected in muscle.

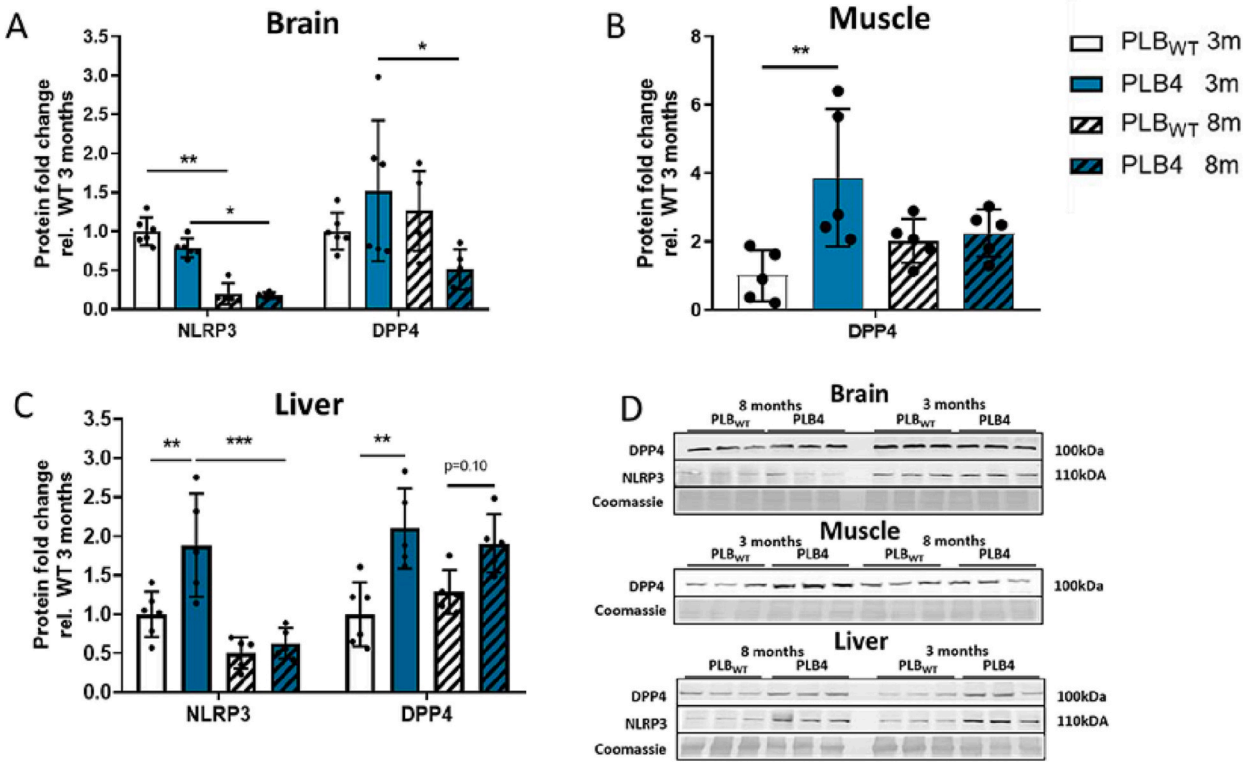

Fig. 6. Effect of ageing on the inflammasome in PLB$_{WT}$ and PLB4 mice. Western blot quantification of protein expression of NLRP3 and DPP4 in insulin-stimulated (A) brain, (B) muscle and (C) liver of 3- and 8-month-old PLB$_{WT}$ and PLB4 male mice. (D) Representative images of DPP4 and NLRP3 in the brain, muscle and liver. NLRP3 and DPP4 were normalised to Coomassie total protein and data expressed as fold change relative to 3-month-old PLB$_{WT}$ ± SD, and analysed using two-way ANOVAs, followed by Tukey's multiple comparison test. *$p < 0.05$, **$p < 0.01$, ***$p < 0.001$. PLB$_{WT}$ 3 months ($n = 6$), PLB4 3 months ($n = 6$), PLB$_{WT}$ 8 months ($n = 5$), PLB4 8 months ($n = 5$). For full statistical results, see Supplementary Tables.

3.7. DPP4 protein levels in brain and peripheral tissues

Next, we assessed the incretin regulator DPP4, which is dysregulated in states of inflammation and in diabetes. DPP4 protein levels were significantly increased in the muscle (interaction: F (1, 16) = 6.396; p = 0.0223, genotype: F (1, 16) = 8.758; p = 0.0092, PLB4 3 months vs. WT 3 months: p = 0.0065), and liver (genotype: F (1, 17) = 23.75; p = 0.0001, PLB4 3 months vs. WT 3 months: p = 0.0016) of 3-month-old PLB4 animals, while only approaching significance for brain tissue (but note age x genotype interaction: F (1, 18) = 6.929; p = 0.0169, PLB4 3 months vs. WT 3 months: p = 0.10, Fig. 6A). Liver DPP4 also approached significance in 8-month-old PLB4s compared to their age-matched WT controls (p = 0.10, Fig. 6C). Furthermore, we observed an age-related decline in brain DPP4 levels in 8-month-old PLB4s compared to 3-months-old (p = 0.0378), which was not observed in peripheral tissues, and not seen in WT controls (Fig. 6A). Proposed interactions between insulin signalling, glucose regulation, ER stress and inflammation pathways in the three tissues investigated have been summarised in Fig. 8.

3.8. Correlation analysis

To confirm potential connections between molecular parameters identified, and to seek indicators for causal links between pathways involved in both AD and T2D pathologies, correlation analyses of markers examined were performed. Data were pooled from 3- and 8-month-old insulin-stimulated animals to determine generic correlations between all parameters measured, independent of age for each genotype (WT; n = 11 and PLB4; n = 11, separately). After confirming data normality, a multi-factorial correlation analysis was conducted using Pearson's correlation coefficient (r- value) to determine associations between variables. Analysis was performed using the average of biological replicates with a single technical data point per animal within each tissue separately first, followed by between tissue testing. Correlation data were plotted as heatmaps, with blue indicating positive and red indicating negative correlations (Fig. 7). Particular emphasis was given to the emergence of clusters of associated cellular proxies, their functional relationships and their differences between genotypes and tissues rather than probing for individual significances. Further statistical details, alongside plots of r- and p-values, can be found in the Supplementary Figs. 2–4.

3.8.1. Brain

Correlation analysis between markers of APP processing, ER stress, insulin signalling, glucose metabolism and inflammation were performed for protein and gene expression data obtained from brain tissue of WT and PLB4 mice (Fig. 7A & D). Differing correlation patterns were observed between genotypes for markers associated with cellular pathology, thus attributable to neuronal *h*BACE1 expression and subsequent amyloidogenic APP processing in PLB4 mice.

No associations between APP processing and ER stress were evident in WT animals. However, insulin signalling correlated positively (blue: p-Akt and BiP) as well as negatively (red: p-Akt and p-eIF2α) with ER stress indicating a mutual relationship, likely affected by age-related changes specifically in WT mice (see Fig. 7A). In contrast, APP misprocessing (monomeric Aβ, sAPPα and sAPPβ) correlated with ER stress and the inflammasome in PLB4s, suggesting that the initial increase in amyloidogenic processing (3 months) and subsequent shift in APP

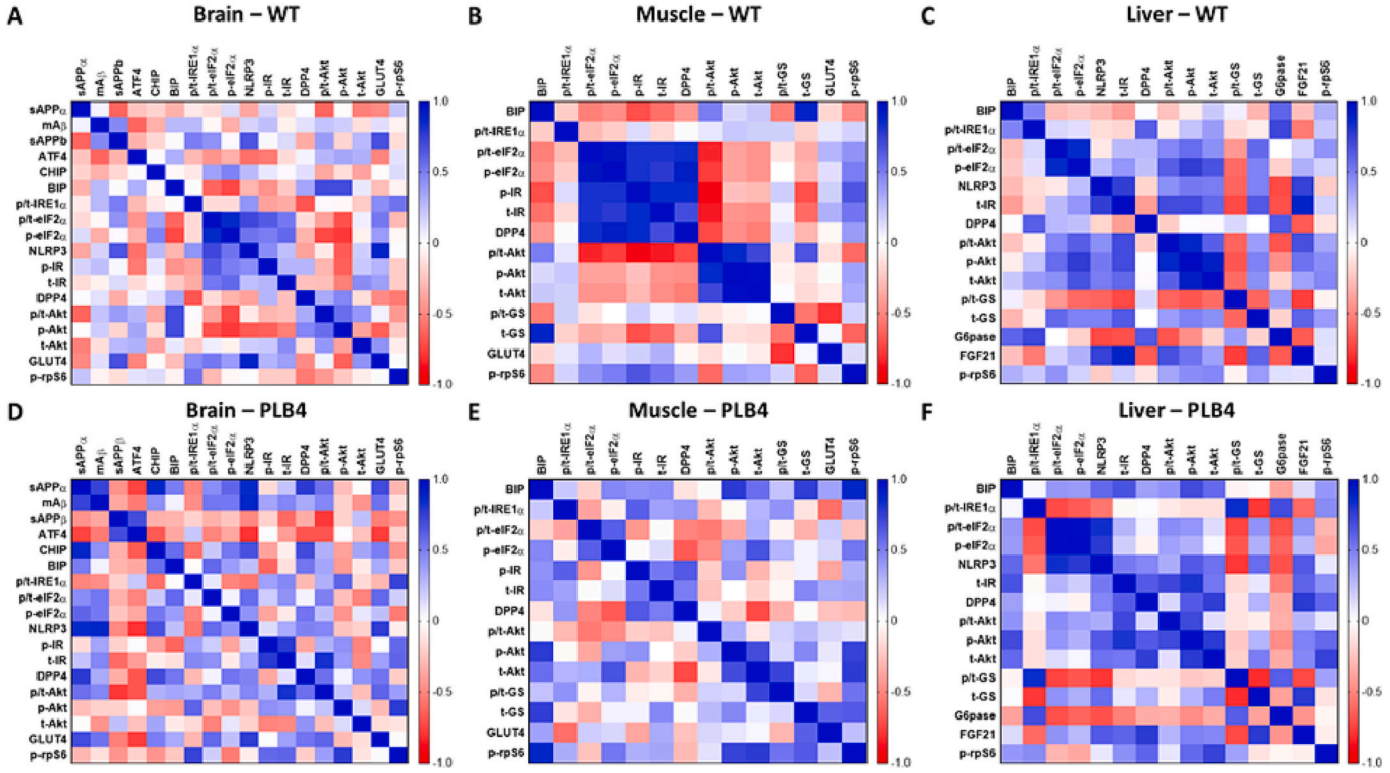

Fig. 7. Within-genotype correlation analysis of protein and gene expression markers for APP processing, ER stress, insulin signalling, glucose regulation and the inflammasome. Correlation analysis was performed for PLB_{WT} and PLB4 separately to identify genotype specific correlations between each pathway regardless of age. Correlation analysis between insulin signalling, glucose metabolism, the inflammasome, ER stress and APP processing in insulin-stimulated (A) brain, (B) muscle and (C) liver tissue of PLB_{WT} mice and (D) brain, (E) muscle and (F) liver of PLB4 mice. Positive correlations are shown by increased intensity in blue (1), with negative correlations determined by increased red intensity (−1) and no correlation identified in white (0). Data underwent Z-score transformation to allow for comparisons between datasets, and data were assessed for normal distribution using D'Agostino & Pearson normality test, followed by Pearson's correlation analysis. For all data, $p < 0.05$ was considered significant. PLB_{WT} (n = 11), PLB4 (n = 11). (For interpretation of the references to colour in this figure legend, the reader is referred to the web version of this article.)

processing (sAPPα and sAPPβ at 8 months) increased cellular stress and inflammation in the brain (Fig. 7D).

Interestingly, no correlations were observed between APP processing and insulin signalling (IR, Akt) in PLB4 mice, suggesting that *h*BACE1 expression and subsequent APP misprocessing does not impair brain insulin signalling. Only sAPPα positively correlated with GLUT4 and DPP4, indicative of reduced glucose transport and homeostasis as a consequence of *h*BACE1 expression (Fig. 7D).

3.8.2. Muscle

Analysis of ER stress, inflammation, insulin signalling, and glucose metabolism in muscle tissue showed striking genotype differences in associations between these cellular pathways (Fig. 7B & E). ER stress and insulin signalling were strongly correlated in WT animals (e.g., p-eIF2α with IRs, Fig. 7B). However, in PLB4 mice there was a clear disconnect between insulin signalling and ER stress, with no corresponding distinct clusters evident (Fig. 7E). Further inspection of DPP4 correlations showed distinct genotype differences, where DPP4 regulation in WTs had strong positive (blue: p/t-eIF2α and p-eIF2α) correlations with ER stress and both positive (blue: p-IR and t-IR) and negative correlations (red: p/t-Akt) with insulin signalling. In contrast, in PLB4 mice DPP4 had moderate negative correlation with ER stress (p-eIF2α) and both moderate negative and positive correlations with IR signalling (p-IR and t-Akt, respectively), indicating dissociations between inflammation, insulin signalling and metabolic cascades in muscle associated with the PLB4 metabolic phenotype (Fig. 7B & E).

3.8.3. Liver

Correlation analysis was next performed for protein and gene expression data obtained from liver tissue of WT and PLB4 mice (Fig. 7C & F). Clustering analysis indicated that ER stress had moderate positive correlations with insulin signalling in WT animals (p-eIF2α with p-Akt), which again is likely an association between impaired cellular stress and metabolic dysfunction with ageing (Fig. 7C). PLB4s however, did not display these correlation patterns indicating dissociations between cellular stress and impaired insulin signalling (Fig. 7F). Subtle positive and negative correlations were found between glucose metabolism and cellular stress in WT animals (G6Pase with IRE1α), however, *h*BACE1 expression in PLB4 mice altered this profile slightly where stronger connections between ER stress and glucose metabolism were observed (GS with IRE1α and eIF2α, and G6Pase with IRE1α), suggesting that increased ER stress may affect liver glucose metabolism, or vice versa; a result of neuronal *h*BACE1 expression (Fig. 7F).

Correlations between the inflammasome, insulin signalling, and glucose metabolism were moderately different between genotypes. The NLRP3 inflammasome showed similar correlation profiles in WT and PLB4s where NLRP3 positively (blue) correlated with insulin signalling (WT: t-IR, PLB4: p-Akt) and negatively with glucose metabolism (red: p/t-GS and G6Pase). Interestingly, and in contrast to muscle, DPP4 did not correlate with insulin signalling but correlated positively and negatively with glucose metabolism (G6Pase and FGF21, respectively) in WT mice, indicating tissue-specific differences in these signalling cascades associated with ageing. In PLB4 mice DPP4 did however correlate positively with both insulin signalling and glucose metabolism (e.g., t-Akt and FGF21), an effect also evident in muscle tissue, but not in the brain (Fig. 7C & F). These data indicate that *h*BACE1 expression alters the link between inflammation, insulin signalling and glucose regulation that occurs under normal physiological conditions and is specific to different tissues, with distinct (early) changes in the periphery that are not evident in the brain.

3.8.4. Correlations between brain and liver

Between-tissue correlation analysis was performed for specific markers of interest to determine whether pathways assessed matched between tissues. No significant correlations in insulin signalling, glucose metabolism or ER stress markers were observed between brain, liver and muscle tissue in PLB4 mice (data not shown). However, a significant positive correlation between brain and liver NLRP3 was found in PLB4 mice only, suggesting that *h*BACE1 expression may cause a more generalised change in the inflammasome response of both tissues (Supplementary Fig. 4).

4. Discussion

BACE1 plays a critical role in the development of AD and its pathophysiology, and also in the development of T2DM associated with AD. Here, we built on our previous work to further characterise the comorbid AD-T2DM phenotype and explore pathways regulated by BACE1 involved in amyloid pathogenesis and metabolic dysregulation in 3- and 8-month-old male PLB4 mice.

4.1. *h*BACE1 expression results in APP misprocessing in the brain

Our original work reported that the knock-in of *h*BACE1 resulted in altered APP processing in PLB4 mice (Plucińska et al., 2014). Also, in line with our recent report, we found that 8-month-old PLB4 mice had elevated levels of FL-APP and lower sAPPα (Dekeryte et al., 2021). No age-related changes were observed in APP processing in wild-type animals, while an increase in monomeric Aβ was detected in 3-month-old PLB4 animals which was subsequently lost with age. Furthermore, sAPPα was lower in 8-month-old PLB4s compared to 3-month-old animals, indicating distinct genotype- and age- dependent changes in APP brain processing. Since sAPPα has multiple beneficial effects on neurons, for example restores defects in plasticity and spatial learning and memory, decreased levels of sAPPα may contribute to impaired learning and memory previously reported in the PLB4 mouse (Habib et al., 2017; Plucińska et al., 2014).

4.2. *h*BACE1 results in a T2DM-like phenotype independent of brain insulin receptor signalling

We confirmed here that the neuron-specific *h*BACE1 knock-in mouse displays T2DM-like symptoms including elevated fasting blood glucose, and impaired glucose tolerance evident from 3 months of age which is sustained in 8-month-old PLB4 male mice. Contrary to our previous work, insulin receptor protein levels were not significantly affected in the brain of 3- or 8-month-old PLB4 male mice, however, it should be noted that animals here received insulin stimulation prior to tissue harvest, a key factor modulating insulin-associated pathways (Plucińska et al., 2016).

Of major interest is the disconnect between pathological APP-processing at 3 months and brain insulin signalling. *h*BACE1 expression and subsequent mAβ and sAPPβ production did not alter IR levels or downstream mechanisms, indicating that pathological APP processing does not dysregulate IR signalling in the brain of young PLB4 mice. Recently, Molina-Fernández et al., 2022 proposed that mAβ indeed does not impair insulin signalling but binds to and activates IRs and downstream mechanisms to regulate glucose uptake and transport in neuroblastoma cells. Conversely, sAPPβ has been implicated in impaired peripheral insulin signalling in BACE1 KO mice. However, it should be noted that these studies examined the direct actions of exogenous sAPPβ in skeletal muscle, and not intrinsically elevated sAPPβ in the brain (Botteri et al., 2018). Despite increased brain sAPPβ levels in older PLB4 mice, peripheral impaired metabolism did not worsen, suggesting the diabetic-like pathology of PLB4 mice may not be driven by APP misprocessing. Furthermore, hyperglycaemia and peripheral insulin resistance have been implicated in reduced APP metabolism and increased cerebrospinal fluid (CSF) sAPPβ, suggesting that hyperglycaemia may have contributed to the increased sAPPβ observed (Hoscheidt et al., 2016; Yang et al., 2013). Here, in PLB4 mice positive correlations were observed between brain GLUT4 and sAPPα, suggesting that reduced non-pathogenic APP processing may contribute to reduced brain glucose

metabolism and the overall hyperglycaemia observed. On the other hand, in states of insulin deficiency, brain BACE1 and full-length APP were upregulated in the 5XFAD APP over-expression mouse model, indicating that a lack of insulin may directly affect APP processing (Devi et al., 2012), but not vice versa.

Upon examination of the age-associated disruption in brain insulin signalling and glucose metabolism, it was also evident that these pathways are not affected by neuronal *h*BACE1 expression. Brain rpS6 phosphorylation and GLUT4 levels markedly decreased with age in both groups. GLUT4 levels remained normal despite increased circulating glucose in PLB4 mice, which may result in reduced brain glucose uptake and metabolism as observed in GLUT4 knock-out mice (Rebelos et al., 2021; Reno et al., 2017). Since brain metabolic changes were age- but not genotype-dependent, it provides further evidence that they are not caused by changes in APP processing, as also confirmed by our correlation analysis.

4.3. Peripheral metabolic signalling is disrupted by neuronal hBACE1 expression

Reduced peripheral responses to insulin is an indicator of insulin resistance affecting glucose uptake and gluconeogenesis (Wijesekara et al., 2018), and previous studies have indicated that BACE1 and its metabolites may regulate insulin signalling in peripheral tissues (Botteri et al., 2018; Meakin et al., 2018; Zhang et al., 2012). Here, peripheral insulin signalling was dysregulated, in a tissue dependent manner, in 3-month-old PLB4 mice. Disrupted muscle IR and Akt, alongside normal GLUT4 levels at 3 months of age, which normalised to wild-type levels at 8 months despite sustained hyperglycaemia, suggested insulin receptor desensitisation decreased activation of the insulin signalling pathway and defective glucose uptake (Bryant et al., 2002; Hamilton et al., 2014; Reno et al., 2017).

Conversely, in the liver IR levels did not change in 3-month-old PLB4 mice, however, Akt levels and FGF21 gene expression increased. FGF21 acts as an insulin sensitizer to overcome peripheral insulin resistance induced by fasting to maximize glucose uptake (Fig. 8). Increased downstream Akt signalling and FGF21 expression suggest that the liver is attempting to deal with higher circulating glucose and compensate for an insulin resistant or desensitised state (BonDurant et al., 2017; Markan et al., 2014). Despite an age-related decline in insulin signalling, Akt levels remained elevated in 8-month-old PLB4 mice which coincided with increased G6Pase expression and reduced GS activity, both of which indicate impaired liver function to suppress hepatic gluconeogenesis, or increased glycogen storage (Hatting et al., 2018; Plucińska et al., 2016).

These data suggest that neuronal *h*BACE1 expression leads to peripheral glucose intolerance, caused by different age-dependent mechanisms, whereby 3-month-old PLB4 mice have impaired glucose uptake in muscle, and 8-month-old PLB4 mice have increased hepatic glucose output alongside decreased glycogen production due to increased insulin resistance, impaired insulin signalling, and increased gluconeogenesis despite hyperglycaemia.

4.4. Neuronal hBACE1 disrupts systemic NLRP3 inflammasome responses

Human and *in vivo* studies have indicated that increased circulating glucose and insulin resistance are associated with increased NLRP3 activity (Ringling et al., 2016). Indeed, 3-month-old PLB4 mice displayed increased NLRP3 levels in the liver alongside increased liver DPP4. DPP4 was associated with activation of the NLRP3 inflammasome (Birnbaum et al., 2018), and here we show specific associations between peripheral DPP4, insulin signalling, and glucose metabolism in the liver that are not evident in the brain of PLB4 mice. Therefore, DPP4 may play a critical role in peripheral dysregulated metabolic signalling via activation of the NLRP3 inflammasome.

It is well established that the NLRP3 inflammasome is activated in diseases associated with ageing, including AD and T2DM (Sebastian-Valverde and Pasinetti, 2020). Conversely, here the NLRP3 inflammasome decreased with age (albeit only 8 months was studied which is not considered to be advanced ageing in mice) in the brain and liver of both wild-type and PLB4 animals. Changes in peripheral glycolysis (increased GS phosphorylation) have been shown to reduce NLRP3 activation (Meyers and Zhu, 2020). Hence, responses of the NLRP3 inflammasome may be a direct effect of age-related changes in glycolytic flux, which needs to be considered when interpreting changes in NLRP3 expression at the protein level.

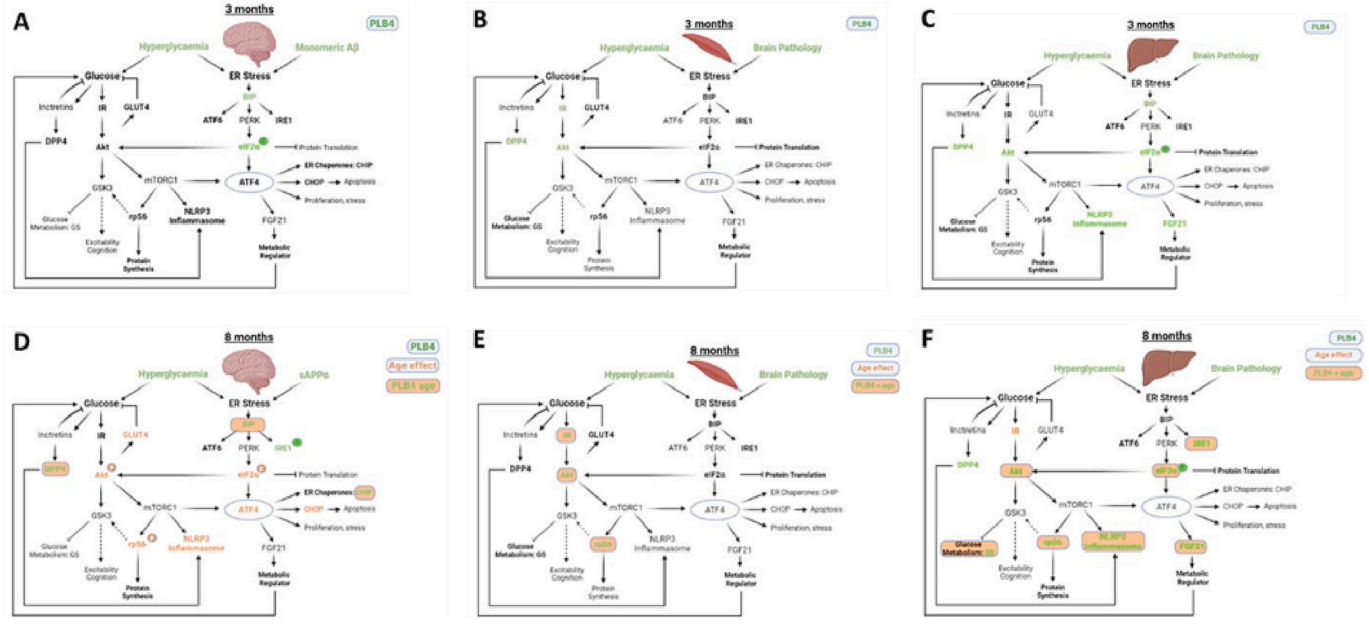

Fig. 8. Illustration of ER stress and metabolic pathways examined in (A, D) brain, (B, E) muscle and (C, F) liver of PLB_{WT} and PLB4 mice and suggested associations between these signalling cascades. Markers highlighted in bold were measured, green: genotype specific changes for PLB4 mice, orange: overall age associated changes and green in orange box: age effect specific to PLB4 mice. (For interpretation of the references to colour in this figure legend, the reader is referred to the web version of this article.)

4.5. Brain and hepatic ER stress responses in PLB4 mice

Increases in the ER stress response and subsequent activation of the unfolded protein response (UPR) are a common feature of both AD and T2D (Koss and Platt, 2017; Özcan et al., 2006). PERK activation is one of the first ER responses activated to promote ER adaptation, and results in downstream eIF2α phosphorylation to lower the overall protein load (Fig. 8; Pandey et al., 2019a). Increased BIP and eIF2α phosphorylation were evident in both the brain and liver from 3 months in PLB4 mice and correlated with altered brain APP processing and dysregulated glucose metabolism. This may indicate an initial adaptive ER stress response to increased amyloidogenic APP processing and impaired peripheral metabolic signalling (Pandey et al., 2019a; Stefani et al., 2021). Indeed, higher levels of brain BIP and phosphorylated eIF2α protein have been observed in cortical neurons in an APP/PS1 mouse (Barbero-Camps et al., 2014; Costa et al., 2013). Decreased eIF2α phosphorylation improved hepatic metabolism and insulin action in diabetic rats, indicating a role for the ER response in impaired hepatic glucose metabolism observed in PLB4 animals (Pandey et al., 2019b).

Brain ER stress responses remained activated at 8 months of age (BIP and eIF2a, but also IRE1a), while monomeric Aβ normalised, suggesting that amyloidogenic processing may have peaked around 3 months and is then successfully compensated for by increased activation of the ER stress response (Hoozemans et al., 2012). Furthermore, hepatic IRE1α activation increased in 8-month-old PLB4 mice, which correlated with gluconeogenic activity (increased GS activation and G6Pase, and decreased FGF21) (Huang et al., 2019). Lee and Ozcan (2014) have shown that suppressed IRE1 activity reduced hepatic gluconeogenesis. Interestingly, the PERK pathway is subject to negative feedback inhibition to restore metabolic homeostasis, therefore, decreased hepatic eIF2-a phosphorylation in 8-month-old PLB4s may be a compensatory mechanism in response to chronic hyperglycaemia, and may explain why PLB4 animals do not become more glucose intolerant with age (Cnop et al., 2017).

5. Conclusions

Peripheral post-insulin receptor signalling, and glucose metabolism were dysregulated early in PLB4 mice alongside brain APP misprocessing suggesting that Aβ production may lead to chronic metabolic dysregulation (Fig. 8). However, monomeric Aβ levels then normalised with age while APP processing overall declined. As the metabolic phenotype did not change, this suggests that compensatory neuronal mechanisms may be at work. Indeed, BIP and eIF2α responses may help to suppress APP processing, while liver FGF21 protein levels may have prevented progression of hyperglycaemia. Future work needs to clarify whether metabolic anomalies are due to other substrates regulated by *h*BACE, and/or highly localised (hypothalamic?) actions of APP and its metabolites.

Overall, our data propose a complex interplay between neuron-specific *h*BACE1 expression with neuronal APP misprocessing associated with early ER stress and inflammation and sustained peripheral (but not CNS) disturbances in insulin signalling and glucose metabolism. As phenotypes of the PLB4 mouse did not progress with age, this provides evidence for compensatory mechanisms, which may offer insights into novel therapeutic targets for AD and T2DM.

Funding

This work was supported by ARUK Project Grant PG2017B-11.

Author contributions

BP, MD and ZF designed the study; BP and MD provided the financial support. ZF carried out the majority of the experimental work and data analysis, with assistance from LC and RD. ZF wrote the initial manuscript; BP and MD critically revised, commented on and edited the manuscript.

Data availability

Data will be made available on request.

Acknowledgements

The authors would like to acknowledge University of Aberdeen PhD studentship funding to RD, and Alzheimer's Research UK Project grant funding to BP and MD (ARUK-PG2017B-11).

Appendix A. Supplementary data

Supplementary data to this article can be found online at https://doi.org/10.1016/j.nbd.2023.106142.

References

Arnold, S.E., Arvanitakis, Z., Macauley-Rambach, S.L., Koenig, A.M., Wang, H.Y., Ahima, R.S., Craft, S., Gandy, S., Buettner, C., Stoeckel, L.E., Holtzman, D.M., Nathan, D.M., 2018. Brain insulin resistance in type 2 diabetes and Alzheimer disease: concepts and conundrums. Nat. Rev. Neurol. 14 (3) https://doi.org/10.1038/nrneurol.2017.185.

Back, S.H., Kaufman, R.J., 2012. Endoplasmic reticulum stress and type 2 diabetes. Annu. Rev. Biochem. https://doi.org/10.1146/annurev-biochem-072909-095555.

Bao, H., Liu, Y., Zhang, M., Chen, Z., Zhang, W., Ge, Y., Kang, D., Gao, F., Shen, Y., 2021. Increased β-site APP cleaving enzyme 1-mediated insulin receptor cleavage in type 2 diabetes mellitus with cognitive impairment. Alzheim. Dement. 17 (7), 1097–1108. https://doi.org/10.1002/alz.12276.

Barbero-Camps, E., Fernández, A., Baulies, A., Martinez, L., Fernández-Checa, J.C., Colell, A., 2014. Endoplasmic reticulum stress mediates amyloid β neurotoxicity via mitochondrial cholesterol trafficking. Am. J. Pathol. https://doi.org/10.1016/j.ajpath.2014.03.014.

Birnbaum, Y., Bajaj, M., Yang, H.C., Ye, Y., 2018. Combined SGLT2 and DPP4 inhibition reduces the activation of the Nlrp3/ASC Inflammasome and attenuates the development of diabetic nephropathy in mice with type 2 diabetes. Cardiovasc. Drugs Ther. https://doi.org/10.1007/s10557-018-6778-x.

BonDurant, L.D., Ameka, M., Naber, M.C., Markan, K.R., Idiga, S.O., Acevedo, M.R., Walsh, S.A., Ornitz, D.M., Potthoff, M.J., 2017. FGF21 regulates metabolism through adipose-dependent and -independent mechanisms. Cell Metab. https://doi.org/10.1016/j.cmet.2017.03.005.

Botteri, G., Salvadó, L., Gumà, A., Lee Hamilton, D., Meakin, P.J., Montagut, G., Ashford, M.L.J., Ceperuelo-Mallafré, V., Fernández-Veledo, S., Vendrell, J., Calderón-Dominguez, M., Serra, D., Herrero, L., Pizarro, J., Barroso, E., Palomer, X., Vázquez-Carrera, M., 2018. The BACE1 product sAPPβ induces ER stress and inflammation and impairs insulin signaling. Metab. Clin. Exp. https://doi.org/10.1016/j.metabol.2018.03.005.

Bryant, N.J., Govers, R., James, D.E., 2002. Regulated transport of the glucose transporter GLUT4. Nat. Rev. Mol. Cell Biol. https://doi.org/10.1038/nrm782.

Cnop, M., Toivonen, S., Igoillo-Esteve, M., Salpea, P., 2017. Endoplasmic reticulum stress and eIF2α phosphorylation: the Achilles heel of pancreatic β cells. Mol. Metabol. 6 (9) https://doi.org/10.1016/j.molmet.2017.06.001.

Costa, R.O., Ferreiro, E., Oliveira, C.R., Pereira, C.M.F., 2013. Inhibition of mitochondrial cytochrome c oxidase potentiates Aβ-induced ER stress and cell death in cortical neurons. Mol. Cell. Neurosci. 52. https://doi.org/10.1016/j.mcn.2012.09.005.

Dekeryte, R., Hull, C., Plucińska, K., Khan, S., Kamli-Salino, S., Mody, N., Morrice, N., McLaughlin, C., Gault, V., Platt, B., Delibegovic, M., 2019. Effects of Liraglutide and Fenretinide treatments on the diabetic phenotype of neuronal human BACE1 knock-in mice. Biochem. Pharmacol. https://doi.org/10.1016/j.bcp.2019.05.020.

Dekeryte, R., Franklin, Z., Hull, C., Croce, L., Kamli-Salino, S., Helk, O., Hoffmann, P.A., Yang, Z., Riedel, G., Delibegovic, M., Platt, B., 2021. The BACE1 inhibitor LY2886721 improves diabetic phenotypes of BACE1 knock-in mice. Biochim. Biophys. Acta Mol. basis Dis. https://doi.org/10.1016/j.bbadis.2021.166149.

Dempsey, C., Rubio Araiz, A., Bryson, K.J., Finucane, O., Larkin, C., Mills, E.L., Robertson, A.A.B., Cooper, M.A., O'Neill, L.A.J., Lynch, M.A., 2017. Inhibiting the NLRP3 inflammasome with MCC950 promotes non-phlogistic clearance of amyloid-β and cognitive function in APP/PS1 mice. Brain Behav. Immun. https://doi.org/10.1016/j.bbi.2016.12.014.

Devi, L., Alldred, M.J., Ginsberg, S.D., Ohno, M., 2012. Mechanisms underlying insulin deficiency-induced acceleration of β-amyloidosis in a mouse model of Alzheimer's disease. PLoS One. https://doi.org/10.1371/journal.pone.0032792.

du Sert, N.P., Hurst, V., Ahluwalia, A., Alam, S., Avey, M.T., Baker, M., Browne, W.J., Clark, A., Cuthill, I.C., Dirnagl, U., Emerson, M., Garner, P., Holgate, S.T., Howells, D.W., Karp, N.A., Lazic, S.E., Lidster, K., MacCallum, C.J., Macleod, M., Würbel, H., 2020. The arrive guidelines 2.0: updated guidelines for reporting animal research. PLoS Biol. https://doi.org/10.1371/journal.pbio.3000410.

Fisher, F.M., Maratos-Flier, E., 2016. Understanding the physiology of FGF21. Annu. Rev. Physiol. 78 https://doi.org/10.1146/annurev-physiol-021115-105339.

Ghemrawi, R., Khair, M., 2020. Endoplasmic reticulum stress and unfolded protein response in neurodegenerative diseases. Int. J. Mol. Sci. https://doi.org/10.3390/ijms21176127.

Goodman, C.A., Hornberger, T.A., 2013. Measuring protein synthesis with SUnSET: a valid alternative to traditional techniques? Exerc. Sport Sci. Rev. https://doi.org/10.1097/JES.0b013e3182798a95.

Griffith, C.M., Eid, T., Rose, G.M., Patrylo, P.R., 2018. Evidence for altered insulin receptor signaling in Alzheimer's disease. Neuropharmacology. https://doi.org/10.1016/j.neuropharm.2018.01.008.

Habib, A., Sawmiller, D., Tan, J., 2017. Restoring soluble amyloid precursor protein α functions as a potential treatment for Alzheimer's disease. J. Neurosci. Res. https://doi.org/10.1002/jnr.23823.

Hamilton, D.L., Findlay, J.A., Montagut, G., Meakin, P.J., Bestow, D., Jalicy, S.M., Ashford, M.L.J., 2014. Altered amyloid precursor protein processing regulates glucose uptake and oxidation in cultured rodent myotubes. Diabetologia. https://doi.org/10.1007/s00125-014-3269-x.

Hatting, M., Tavares, C.D.J., Sharabi, K., Rines, A.K., Puigserver, P., 2018. Insulin regulation of gluconeogenesis. Ann. N. Y. Acad. Sci. https://doi.org/10.1111/nyas.13435.

Hoozemans, J.J.M., Van Haastert, E.S., Nijholt, D.A.T., Rozemuller, A.J.M., Scheper, W., 2012. Activation of the unfolded protein response is an early event in Alzheimer's and Parkinson's disease. Neurodegener. Dis. https://doi.org/10.1159/000334536.

Hoscheidt, S.M., Starks, E.J., Oh, J.M., Zetterberg, H., Blennow, K., Krause, R.A., Gleason, C.E., Puglielli, L., Atwood, C.S., Carlsson, C.M., Asthana, S., Johnson, S.C., Bendlin, B.B., 2016. Insulin resistance is associated with increased levels of cerebrospinal fluid biomarkers of Alzheimer's disease and reduced memory function in at-risk healthy middle-aged adults. J. Alzheimers Dis. 52 (4) https://doi.org/10.3233/JAD-160110.

Huang, S., Xing, Y., Liu, Y., 2019. Emerging roles for the ER stress sensor IRE1 in metabolic regulation and disease. J. Biol. Chem. 294 (49), 18726–18741. https://doi.org/10.1074/jbc.REV119.007036.

Hull, C., Dekeryte, R., Koss, D.J., Crouch, B., Buchanan, H., Delibegovic, M., Platt, B., 2020. Knock-in of mutated hTAU causes insulin resistance, inflammation and proteostasis disturbance in a mouse model of frontotemporal dementia. Mol. Neurobiol. https://doi.org/10.1007/s12035-019-01722-6.

Isik, A.T., Soysal, P., Yay, A., Usarel, C., 2017. The effects of sitagliptin, a DPP-4 inhibitor, on cognitive functions in elderly diabetic patients with or without Alzheimer's disease. Diabetes Res. Clin. Pract. https://doi.org/10.1016/j.diabres.2016.12.010.

Ke, Y.D., Delerue, F., Gladbach, A., Götz, J., Ittner, L.M., 2009. Experimental diabetes mellitus exacerbates tau pathology in a transgenic mouse model of Alzheimer's disease. PLoS One 4 (11). https://doi.org/10.1371/journal.pone.0007917.

Kimura, N., 2016. Diabetes mellitus induces Alzheimer's disease pathology: histopathological evidence from animal models. Int. J. Mol. Sci. 17 (4) https://doi.org/10.3390/ijms17040503.

Klemann, C., Wagner, L., Stephan, M., von Hörsten, S., 2016. Cut to the chase: a review of CD26/dipeptidyl peptidase-4's (DPP4) entanglement in the immune system. Clin. Exp. Immunol. https://doi.org/10.1111/cei.12781.

Koss, D.J., Platt, B., 2017. Alzheimer's disease pathology and the unfolded protein response: prospective pathways and therapeutic targets. Behav. Pharmacol. https://doi.org/10.1097/FBP.0000000000000299.

Koss, D.J., Jones, G., Cranston, A., Gardner, H., Kanaan, N.M., Platt, B., 2016. Soluble pre-fibrillar tau and β-amyloid species emerge in early human Alzheimer's disease and track disease progression and cognitive decline. Acta Neuropathol. https://doi.org/10.1007/s00401-016-1632-3.

Lee, J., Ozcan, U., 2014. Unfolded protein response signaling and metabolic diseases. J. Biol. Chem. https://doi.org/10.1074/jbc.R113.534743.

Li, X., Song, D., Leng, S.X., 2015. Link between type 2 diabetes and Alzheimer's disease: from epidemiology to mechanism and treatment. Clin. Interv. Aging. https://doi.org/10.2147/CIA.S74042.

Markan, K.R., Naber, M.C., Ameka, M.K., Anderegg, M.D., Mangelsdorf, D.J., Kliewer, S. A., Mohammadi, M., Potthoff, M.J., 2014. Circulating FGF21 is liver derived and enhances glucose uptake during refeeding and overfeeding. Diabetes. https://doi.org/10.2337/db14-0595.

Meakin, P.J., Harper, A.J., Hamilton, D.L., Gallagher, J., McNeilly, A.D., Burgess, L.A., Vaanholt, L.M., Bannon, K.A., Latcham, J., Hussain, I., Speakman, J.R., Howlett, D. R., Ashford, M.L.J., 2012. Reduction in BACE1 decreases body weight, protects against diet-induced obesity and enhances insulin sensitivity in mice. Biochem. J. https://doi.org/10.1042/BJ20110512.

Meakin, P.J., Mezzapesa, A., Benabou, E., Haas, M.E., Bonardo, B., Grino, M., Brunel, J. M., Desbois-Mouthon, C., Biddinger, S.B., Govers, R., Ashford, M.L.J., Peiretti, F., 2018. The beta secretase BACE1 regulates the expression of insulin receptor in the liver. Nat. Commun. https://doi.org/10.1038/s41467-018-03755-2.

Meyers, A.K., Zhu, X., 2020. The NLRP3 Inflammasome: metabolic regulation and contribution to Inflammaging. Cells 9 (8). https://doi.org/10.3390/cells9081808.

Molina-Fernández, R., Picón-Pagès, P., Barranco-Almohalla, A., Crepin, G., Herrera-Fernández, V., García-Elías, A., Fanlo-Ucar, H., Fernàndez-Busquets, X., García-Ojalvo, J., Oliva, B., Muñoz, F.J., 2022. Differential regulation of insulin signalling by monomeric and oligomeric amyloid beta-peptide. Brain Commun. 4 (5) https://doi.org/10.1093/braincomms/fcac243.

Özcan, U., Cao, Q., Yilmaz, E., Lee, A.H., Iwakoshi, N.N., Özdelen, E., Tuncman, G., Görgün, C., Glimcher, L.H., Hotamisligil, G.S., 2004. Endoplasmic reticulum stress links obesity, insulin action, and type 2 diabetes. Science 306 (5695). https://doi.org/10.1126/science.1103160.

Özcan, U., Yilmaz, E., Özcan, L., Furuhashi, M., Vaillancourt, E., Smith, R.O., Görgün, C. Z., Hotamisligil, G.S., 2006. Chemical chaperones reduce ER stress and restore glucose homeostasis in a mouse model of type 2 diabetes. Science 313 (5790). https://doi.org/10.1126/science.1128294.

Pandey, V.K., Mathur, A., Kakkar, P., 2019a. Emerging role of unfolded protein response (UPR) mediated proteotoxic apoptosis in diabetes. Life Sci. https://doi.org/10.1016/j.lfs.2018.11.041.

Pandey, V.K., Mathur, A., Khan, M.F., Kakkar, P., 2019b. Activation of PERK-eIF2α-ATF4 pathway contributes to diabetic hepatotoxicity: attenuation of ER stress by Morin. Cell. Signal. https://doi.org/10.1016/j.cellsig.2019.03.008.

Patterson, B.W., Elbert, D.L., Mawuenyega, K.G., Kasten, T., Ovod, V., Ma, S., Xiong, C., Chott, R., Yarasheski, K., Sigurdson, W., Zhang, L., Goate, A., Benzinger, T., Morris, J.C., Holtzman, D., Bateman, R.J., 2015. Age and amyloid effects on human central nervous system amyloid-beta kinetics. Ann. Neurol. https://doi.org/10.1002/ana.24454.

Plucińska, K., Crouch, B., Koss, D., Robinson, L., Siebrecht, M., Riedel, G., Platt, B., 2014. Knock-in of human BACE1 cleaves murine APP and reiterates alzheimer-like phenotypes. J. Neurosci. https://doi.org/10.1523/JNEUROSCI.0433-14.2014.

Plucińska, K., Dekeryte, R., Koss, D., Shearer, K., Mody, N., Whitfield, P.D., Doherty, M. K., Mingarelli, M., Welch, A., Riedel, G., Delibegovic, M., Platt, B., 2016. Neuronal human BACE1 knockin induces systemic diabetes in mice. Diabetologia. https://doi.org/10.1007/s00125-016-3960-1.

Rai, R.C., Bagul, P.K., Banerjee, S.K., 2020. NLRP3 inflammasome drives inflammation in high fructose fed diabetic rat liver: effect of resveratrol and metformin. Life Sci. 253 https://doi.org/10.1016/j.lfs.2020.117727.

Rebelos, E., Rinne, J.O., Nuutila, P., Ekblad, L.L., 2021. Brain glucose metabolism in health, obesity, and cognitive decline—Does insulin have anything to do with it? A narrative review. J. Cli. Med. https://doi.org/10.3390/jcm10071532.

Reno, C.M., Puente, E.C., Sheng, Z., Daphna-Iken, D., Bree, A.J., Routh, V.H., Kahn, B.B., Fisher, S.J., 2017. Brain GLUT4 knockout mice have impaired glucose tolerance, decreased insulin sensitivity, and impaired hypoglycemic counterregulation. Diabetes. https://doi.org/10.2337/db16-0917.

Rheinheimer, J., de Souza, B.M., Cardoso, N.S., Bauer, A.C., Crispim, D., 2017. Current role of the NLRP3 inflammasome on obesity and insulin resistance: a systematic review. Metab. Clin. Exp. https://doi.org/10.1016/j.metabol.2017.06.002.

Ringling, R.E., Gastecki, M.L., Woodford, M.L., Lum-Naihe, K.J., Grant, R.W., Pulakat, L., Vieira-Potter, V.J., Padilla, J., 2016. Loss of Nlrp3 does not protect mice from western diet-induced adipose tissue inflammation and glucose intolerance. PLoS One. https://doi.org/10.1371/journal.pone.0161939.

Rusli, F., Deelen, J., Andriyani, E., Boekschoten, M.V., Lute, C., Van Den Akker, E.B., Müller, M., Beekman, M., Steegenga, W.T., 2016. Fibroblast growth factor 21 reflects liver fat accumulation and dysregulation of signalling pathways in the liver of C57BL/6J mice. Sci. Rep. 6 https://doi.org/10.1038/srep30484.

Sebastian-Valverde, M., Pasinetti, G.M., 2020. The NLRP3 inflammasome as a critical actor in the inflammaging process. Cells 9 (6). https://doi.org/10.3390/cells9061552.

Stefani, I.C., Blaudin de Thé, F.X., Kontoravdi, C., Polizzi, K.M., 2021. Model identifies genetic predisposition of alzheimer's disease as key decider in cell susceptibility to stress. Int. J. Mol. Sci. 22 (21) https://doi.org/10.3390/ijms222112001.

Taylor, H.A., Przemylska, L., Clavane, E.M., Meakin, P.J., 2022. BACE1: more than just a β-secretase. In: Obesity Reviews, Vol. 23. John Wiley and Sons Inc. https://doi.org/10.1111/obr.13430. Issue 7.

Tezze, C., Romanello, V., Sandri, M., 2019. FGF21 as modulator of metabolism in health and disease. Front. Physiol. 10 (MAR) https://doi.org/10.3389/fphys.2019.00419.

Vassar, R., Bennett, B.D., Babu-Khan, S., Kahn, S., Mendiaz, E.A., Denis, P., Teplow, D.B., Ross, S., Amarante, P., Loeloff, R., Luo, Y., Fisher, S., Fuller, J., Edenson, S., Lile, J., Jarosinski, M.A., Biere, A.L., Curran, E., Burgess, T., Citron, M., 1999. β-Secretase cleavage of Alzheimer's amyloid precursor protein by the transmembrane aspartic protease BACE. Science. https://doi.org/10.1126/science.286.5440.735.

Wang, Z., Zhang, S., Xiao, Y., Zhang, W., Wu, S., Qin, T., Yue, Y., Qian, W., Li, L., 2020. NLRP3 Inflammasome and inflammatory diseases. Oxidative Med. Cell. Longev. https://doi.org/10.1155/2020/4063562.

Wijesekara, N., Gonçalves, R.A., De Felice, F.G., Fraser, P.E., 2018. Impaired peripheral glucose homeostasis and Alzheimer's disease. Neuropharmacology. https://doi.org/10.1016/j.neuropharm.2017.11.027.

Yang, Y., Wu, Y., Zhang, S., Song, W., 2013. High glucose promotes Aβ production by inhibiting APP degradation. PLoS One 8 (7). https://doi.org/10.1371/journal.pone.0069824.

Zhai, Y., Meng, X., Ye, T., Xie, W., Sun, G., Sun, X., 2018. Inhibiting the NLRP3 inflammasome activation with MCC950 ameliorates diabetic encephalopathy in db/db mice. Molecules. https://doi.org/10.3390/molecules23030522.

Zhang, Y., Zhou, B., Zhang, F., Wu, J., Hu, Y., Liu, Y., Zhai, Q., 2012. Amyloid-β induces hepatic insulin resistance by activating JAK2/STAT3/SOCS-1 signaling pathway. Diabetes. https://doi.org/10.2337/db11-0499.